communications biology

Article

https://doi.org/10.1038/s42003-024-06820-3

Calcium modulates the tethering of BCOR-PRC1.1 enzymatic core to KDM2B via liquid-liquid phase separation

Check for updates

Rui Chen[1,2,7], Feng Shen[1,2,7], Yulong Zhang[2], Mingze Sun[2,3,4], Yan Dong[2,3,4], Yue Yin[5], Chen Su[5], Chao Peng[5], Jinsong Liu[1,2,3,4] ✉ & Jinxin Xu[2,3,4,6] ✉

Recruitment of non-canonical BCOR-PRC1.1 to non-methylated CpG islands via KDM2B plays a fundamental role in transcription control during developmental processes and cancer progression. However, the mechanism is still largely unknown on how this recruitment is regulated. Here, we unveiled the importance of the Poly-D/E regions within the linker of BCOR for its binding to KDM2B. Interestingly, we also demonstrated that these negatively charged Poly-D/E regions on BCOR play autoinhibitory roles in liquid-liquid phase separation (LLPS) of $BCOR^{ANK\text{-}linker\text{-}PUFD}$/$PCGF1^{RAWUL}$. Through neutralizing negative charges of these Poly-D/E regions, Ca^{2+} not only weakens the interaction between BCOR/PCGF1 and KDM2B, but also promotes co-condensation of the enzymatic core of BCOR-PRC1.1 with KDM2B into liquid-like droplet. Accordingly, we propose that Ca^{2+} could modulate the compartmentation and recruitment of the enzymatic core of BCOR-PRC1.1 on KDM2B target loci. Thus, our finding advances the mechanistic understanding on how the tethering of BCOR-PRC1.1 enzymatic core to KDM2B is regulated.

In eukaryotic cells, gene transcription or expression depends heavily on the conformation of chromatin, which is modulated by DNA methylation or post-translation modification of histone tail via chromatin modifying complexes[1,2]. Among the epigenetic regulators involving in histone modification, polycomb repressive complexes (PRCs) have gained much attention, playing fundamental roles in cellular processes, such as development, carcinogenesis and self-renewal of embryonic stem cells[3–6]. Based on enzymatic activity toward histone proteins, PRCs are mainly composed of two multi-protein complexes named PRC1 and PRC2[7,8]. PRC1 catalyzes the mono-ubiquitination of K119 on histone H2A through the heterodimer of RING1 A/B and PCGF protein[9]. PRC2 is a methyltransferase that methylates K27 on histone H3, performed by its core subunits EZH1/EZH2, EED and SUZ12[10,11].

In addition to possessing E3 ligase activity, RING1-PCGF heterodimer also forms scaffold for PRC1 assembly by recruiting accessory proteins via the C-terminal RAWUL domains[12]. Based on PCGF member (PCGF1-6), mammalian PRC1 complexes have been classified into six groups, PRC1.1-PRC1.6[13]. Canonical PRC1 (cPRC1), containing RING1A/B, PCGF2 or 4, CBX protein and PHC protein[14], is recruited to H3K27me3 enriched site of chromatin through the chromodomain of CBX protein[15]. However, in non-canonical PRC1 (ncPRC1), CBX protein is replaced by RYBP or its homolog YAF2, suggesting that ncPRC1 binds to chromatin independent of the histone mark H3K27me3 deposited by PRC2[15]. In contrast to canonical PRC1, a variety of ncPRC1s are much more active on ubiquitylating histone H2A at Lys119 and repressing gene expression, therefore are fundamental in maintaining mESCs identity[3,16–18].

PRC1.1 is a non-canonical PRC1 that has been well identified as a critical regulator in identity maintenance of ESCs, as well as in solid and hematologic cancers[19–22]. In addition to RING1 A/B protein and PCGF1, PRC1.1 also comprises non-PcG proteins, including KDM2B, BCOR or its homolog BCORL1, SKP1 and RYBP. Although BCOR and BCORL1 are homologous, these two proteins exhibit different expression profile. Different from BCORL1, BCOR is highly expressed in hESCs and many tissues[22,23]. In addition to acting as a tumor suppressor in normal cells, recent studies also showed that BCOR in PRC1.1 is essential for leukemogenesis and proliferation of prostate cancer[24,25].

[1]Division of Life Sciences and Medicine, University of Science and Technology of China, Hefei, 230026, China. [2]State Key Laboratory of Respiratory Disease, Guangzhou Institutes of Biomedicine and Health, Chinese Academy of Sciences, Guangzhou, 510530, China. [3]Guangdong Provincial Key Laboratory of Biocomputing, Guangzhou Institutes of Biomedicine and Health, Chinese Academy of Sciences, Guangzhou, 510530, China. [4]China-New Zealand Joint Laboratory on Biomedicine and Health, Guangzhou, 510530, China. [5]National Facility for Protein Science in Shanghai, Shanghai Advanced Research Institute, Chinese Academy of Science, Shanghai, 201210, China. [6]Key Laboratory of Regenerative Biology, Guangzhou Institutes of Biomedicine and Health, Chinese Academy of Sciences, Guangzhou, 510530, China. [7]These authors contributed equally: Rui Chen, Feng Shen. ✉e-mail: liu_jinsong@gibh.ac.cn; xu_jinxin@gibh.ac.cn

Via the CxxC domain of KDM2B that specifically binds to the non-methylated CpG dinucleotide, PRC1.1 can be recruited to CpG islands (CGIs)[26–28]. The importance of PRC1.1 regulating gene expression was evident by the fact that CGIs are frequently enriched in promoters of ~70% of mammalian genes, including housekeeping genes, as well as genes that are active in early developmental stages[26,29,30]. To recruit enzymatic core RING1-PCGF1, KDM2B must cooperate with BCOR or BCORL1. Mutations on BCOR/BCORL1 unlinking PRC1.1 core to KDM2B have been demonstrated contributing to the progression and poor prognosis of acute myeloid leukemia (AML)[24,31]. Structural studies on BCORL1-PRC1.1 revealed that the leucine rich repeats (LRRs) domain of KDM2B binds to the interface formed by heterodimer of C-terminal PUFD domain of BCORL1 and RAWUL domain of PCGF1[32]. Conversely, biochemical data showed that heterodimer of $BCOR^{PUFD}$ and $PCGF1^{RAWUL}$ is not sufficient to interact with KDM2B, while the linker region between ANK and PUFD domain of BCOR is indispensable for its binding to KDM2B[22,32,33].

Interestingly, several studies had revealed that, almost all of CGI are highly occupied by KDM2B, but only a fraction of them are enriched for RING1B[27,28,34]. This implies that KDM2B recruiting enzymatic core of PRC1.1 to non-methylated CpG islands is tightly controlled. Compared to lowly expressed BCORL1, the importance of BCOR in PRC1.1 has been well established in cell fate decision and cancer development[19,31,35]. However, mechanism details are still largely unknown on how BCOR links the enzymatic core of PRC1.1 to KDM2B. In this study, we constructed a structure model of $BCOR^{ANK\text{-}linker\text{-}PUFD}$/$PCGF1^{RAWUL}$/$KDM2B^{F\text{-}box\text{-}LRRs}$/SKP1 using integrated methods, including X-ray crystallography, XL-MS and SAXS. Our structural and biochemical studies revealed that electrostatic interactions, contributed by Poly-D/E regions on linker of BCOR and positively charged residues on the F-box and LRRs of KDM2B, are essential for BCOR/PCGF1 interacting with KDM2B/SKP1. This interaction can be weakened by Ca^{2+} through neutralizing the Poly-D/E regions. Intriguingly, Ca^{2+} also induces the liquid-liquid phase separation of $BCOR^{ANK\text{-}linker\text{-}PUFD}$/$PCGF1^{RAWUL}$, leading to condensation of enzymatic core of BCOR-PRC1.1 together with KDM2B. Taken together, this study suggests that the tethering of BCOR-PRC1.1 enzymatic core to KDM2B may be modulated by Ca^{2+}.

Results

Poly-D/E on the linker region of BCOR is critical for its association with KDM2B

The mechanism for BCORL1 binding to KDM2B was reported that heavily relies on E1664 of $BCORL1^{PUFD}$ domain[32]. However, for the homologous BCOR, the mechanism on its binding to KDM2B remains unknown, due to the substitution of the critical residue E1664 by L1705 on the PUFD domain of BCOR. Previously, Co-IP experiments showed that the linker region connecting ANK and PUFD domain may be solely responsible for BCOR association with KDM2B[22]. However, more recently, Wang and colleagues failed to detect association between $BCOR^{linker}$ and KDM2B using biolayer interferometry (BLI)[33]. Although contradicting in the role of linker region in BCOR association with KDM2B, both groups agreed that ANK contributes moderately to BCOR binding to KDM2B. To confirm the contribution made by ANK domain and the linker region, we performed Isothermal Titration Calorimetry (ITC) assays to determine the interaction between $BCOR^{ANK\text{-}linker}$ and $KDM2B^{F\text{-}box\text{-}LRRs}$/SKP1 dimer ($KDM2B^{F\text{-}box\text{-}LRRs}$ indicates a truncation of KDM2B containing C-terminal F-box domain and LRR repeats domain) (Fig. 1A–C). Interestingly, we failed to detect interaction between $BCOR^{ANK\text{-}linker}$ and KDM2B/SKP1 dimer with buffer containing 150 mM NaCl, whereas this binding was detected with a K_d value of $6.35 \pm 2.01\ \mu M$ when concentration of NaCl in buffer was decreased to 50 mM (Fig. 1C). Then, we tested whether the interaction between $BCOR^{ANK\text{-}linker\text{-}PUFD}$/$PCGF1^{RAWUL}$ dimer and KDM2B/SKP1 dimer could be detected in buffer containing 150 mM NaCl. As shown in Fig. 1D, $BCOR^{ANK\text{-}linker\text{-}PUFD}$/$PCGF1^{RAWUL}$ dimer exhibits strong interaction with KDM2B/SKP1 dimer with a K_d value of $0.20 \pm 0.03\ \mu M$.

$BCOR^{ANK\text{-}linker}$ binding to KDM2B can be disrupted by increasing salt concentration, which indicates that the interaction is mainly electrostatic. Upon a closer look at the linker sequence within BCOR, three regions enriched with negatively charged residues (Poly-D/E) were identified. Hereinafter, the three Poly-D/E regions are named Poly-D/E^{1st} (residues 1591–1593), Poly-D/E^{2nd} (residues 1607–1611) and Poly-D/E^{3rd} (residues 1624–1631), respectively (Fig. 1A). To further explore the roles of these Poly-D/E regions in BCOR for binding to KDM2B, Co-IP experiments were performed with Flag-tagged BCOR (wild type or mutant), PCGF1, KDM2B and SKP1 over-expressed in HEK293T cells. As shown in Fig. 1E, F, BCOR binding to KDM2B or SKP1 was apparently impaired by mutating D/E residues on three Poly-D/E regions to Ala, implying the importance of the Poly-D/E regions for BCOR binding to KDM2B.

To explore which Poly-D/E region is involved in BCOR binding to KDM2B via electrostatic interactions, here, we constructed several truncations for the linker of BCOR (Fig. 1B), and ITC assays were used to measure the affinities of heterodimers of these truncations and $PCGF1^{RAWUL}$ binding to KDM2B/SKP1 with buffer containing 150 mM NaCl. The results showed that the binding affinity of $BCOR^{N1591}$ / $PCGF1^{RAWUL}$ to KDM2B/SKP1 was $0.24 \pm 0.05\ \mu M$, which is comparable to that of $BCOR^{ANK\text{-}linker\text{-}PUFD}$/$PCGF1^{RAWUL}$ dimer (Fig. 1D). This suggested that the ANK domain is not critical for BCOR binding to KDM2B. Then, we determined the affinity of $BCOR^{N1594}$ /$PCGF1^{RAWUL}$ binding to KDM2B/SKP1 to be $0.25 \pm 0.06\ \mu M$, suggesting Poly-D/E^{1st} (1591–1593) is not required for BCOR binding to KDM2B (Fig. 1D). The determined K_d values for $BCOR^{N1607}$/$PCGF1^{RAWUL}$ dimer, $BCOR^{N1612}$ /$PCGF1^{RAWUL}$ dimer and $BCOR^{N1624}$ /$PCGF1^{RAWUL}$ dimer to KDM2B/SKP1 are $0.27 \pm 0.03\ \mu M$, $0.85 \pm 0.09\ \mu M$ and $5.93 \pm 1.73\ \mu M$, respectively (Fig. 1D). When Poly-D/E^{3rd} region was further truncated to just preceding the PUFD domain, the interaction between $BCOR^{PUFD}$/$PCGF1^{RAWUL}$ and KDM2B/SKP1 could not be detected (Fig. 1D). These results suggest that Poly-D/E^{2nd} (1607–1611), Poly-D/E^{3rd} (1624–1631), as well as residues between them, contribute to BCOR binding to KDM2B.

Crystal structure reveals that the conserved NPPGP motif in linker region is also involved in BCOR binding to KDM2B

To explore the detailed mechanism on how BCOR binds to KDM2B, we performed structural studies on BCOR/PCGF1 in complex with KDM2B/SKP1 or LRR repeats alone of KDM2B ($KDM2B^{LRRs}$). Eventually, we successfully obtained high quality crystals for $BCOR^{N1607}$/$PCGF1^{RAWUL}$/$KDM2B^{LRRs}$ heterotrimer. The crystal structure was determined to resolution of 2.2 Å in space group $P4_32_12$ with one heterotrimer in the asymmetric unit.

For the linker of $BCOR^{N1607}$, the electron density is only visible for residues from N1619 to D1625, with electron density missing for residues E1607–A1618 and Q1626-S1634. In the crystal structure, N1619–D1625 occupies a narrow cavity formed by the first and second LRR motif of $KDM2B^{LRRs}$. This binding is stabilized by both hydrophobic and hydrophilic interactions. Key residues contributing to hydrophobic interactions include P1620 and P1621 from BCOR, and P1115/L1118/W1143 from KDM2B. Hydrophilic interactions include hydrogen bond formed by main chain carbonyl of N1619 from BCOR and side chain nitrogen of W1143 from KDM2B (Fig. 2A). These interactions observed in the crystal structure corroborate well with our affinity determination. Residues between Poly-D/E^{2nd} (1607–1611) and Poly-D/E^{3rd} (1624–1631) contribute to BCOR binding with KDM2B/SKP1, as $BCOR^{N1612}$/$PCGF1^{RAWUL}$ dimer exhibited stronger KDM2B/SKP1 binding capacity than that of $BCOR^{N1624}$/ $PCGF1^{RAWUL}$ (Fig. 1D). To further confirm that these interactions revealed in crystal structure contribute to BCOR binding to KDM2B, we constructed mutations on P1620 and P1621 of BCOR, and W1143 of KDM2B. The results clearly showed that binding affinity of $BCOR^{ANK\text{-}linker\text{-}PUFD}$/$PCGF1^{RAWUL}$ dimer and KDM2B/SKP1 dimer was reduced by P1620A/P1621A double mutation of BCOR or W1143A mutation of KDM2B (Fig. 2B). Sequence alignment showed that, ^{1619}NPPGP^{1623} motif on linker of BCOR is conserved among species from zebrafish to human (Fig. 2C). Taken together, these data revealed that the conserved NPPGP motif preceding the Poly-D/E^{3rd} (1624–1631) also contributes to BCOR association with KDM2B.

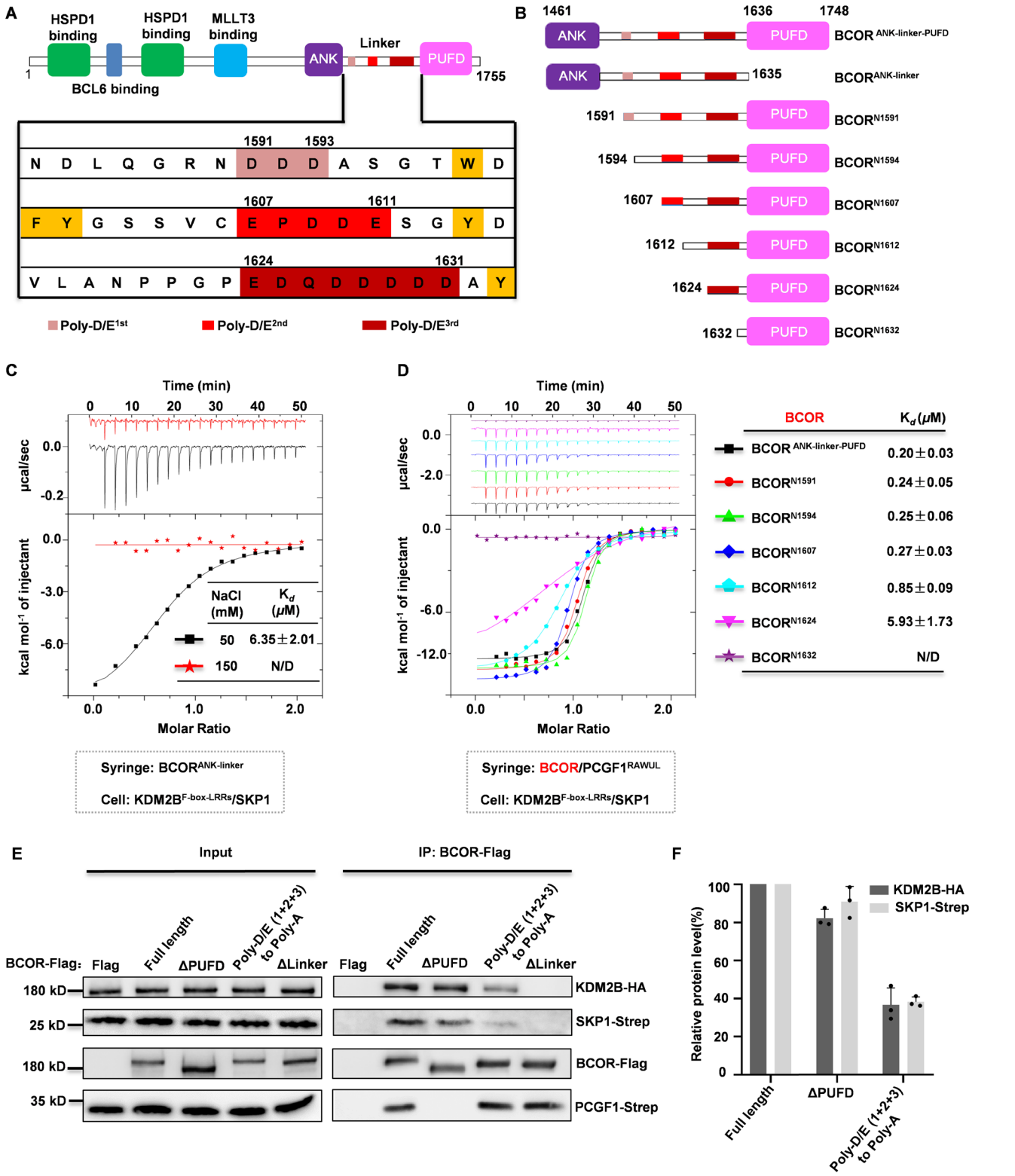

Fig. 1 | Determination of the role of Poly-D/E regions on BCOR binding to KDM2B. A Schematic representation of the domain architecture of BCOR. Three Poly-D/E regions on linker are highlighted with light red for Poly-D/E^{1st}, red for Poly-D/E^{2nd}, and dark red for Poly-D/E^{3rd}. **B** Truncations of BCOR used in this study. **C** Binding affinity between BCOR$^{ANK\text{-}linker}$ and KDM2B$^{F\text{-}box\text{-}LRRs}$/SKP1 was measured by ITC with buffer containing 50 mM or 150 mM NaCl. **D** Binding affinity measurement between dimer of PCGF1^{RAWUL}/indicated BCOR truncation and the KDM2B$^{F\text{-}box\text{-}LRRs}$/SKP1 dimer using ITC with buffer containing 150 mM NaCl. N/D: Cannot be determined. For (**C**, **D**), The K_d values are shown as mean ± SD for triplicate experiments. **E** The importance of Poly-D/E regions on the linker of BCOR binding to KDM2B/SKP1 is assessed using Co-IP assay. Expressing plasmids for BCOR (wild or mutant), PCGF1, KDM2B or SKP1, were co-transfected into HEK293T cells. Co-IP was performed with anti-Flag magnetic beads, after 48 h transfection. The western-blotting data is representative of three independent experiments. **F** Relative level of KDM2B-HA or PCGF1-strep protein co-purified with BCOR-Flag as shown in (**E**). Data are represented as mean ± SD for triplicate experiments.

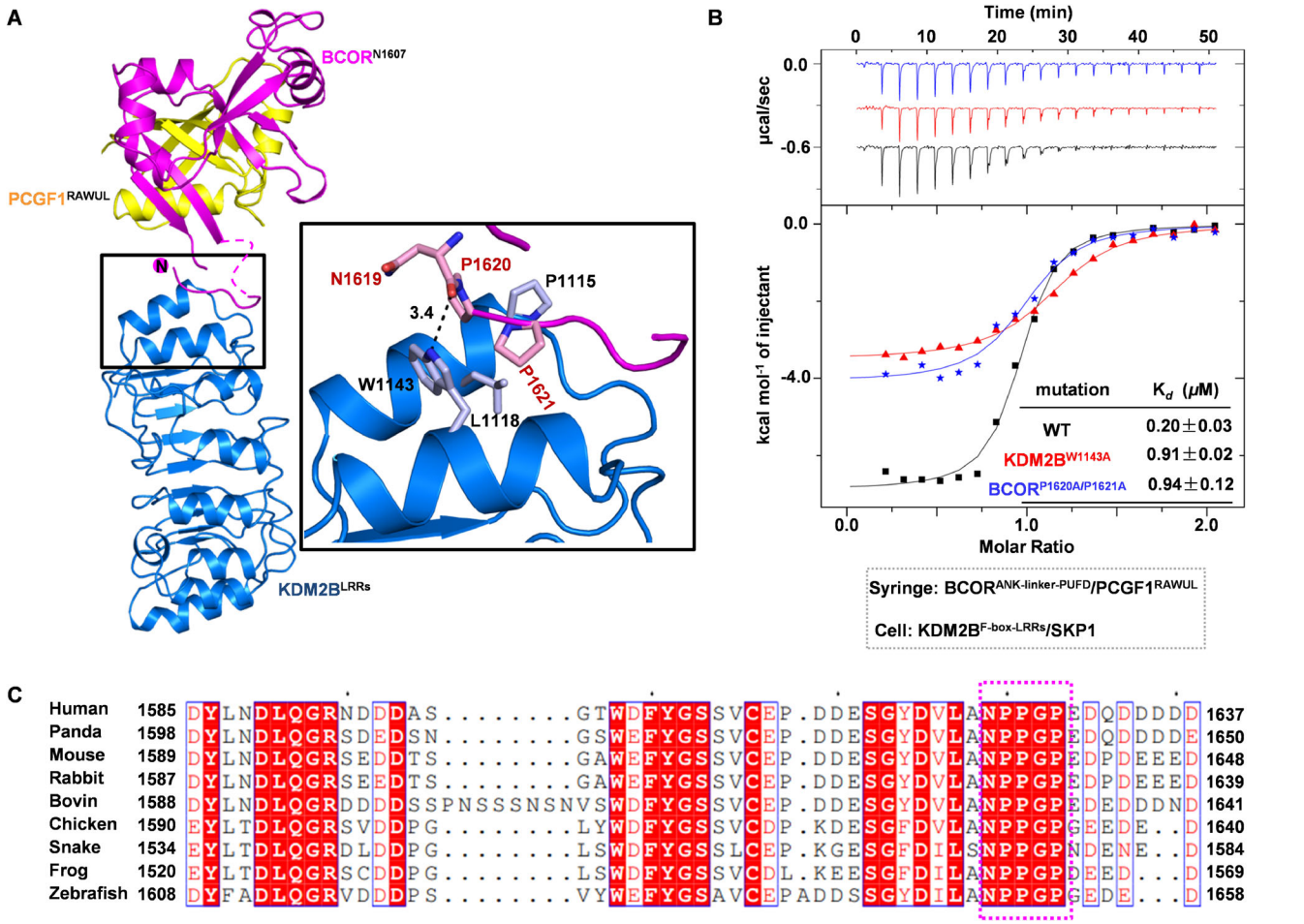

Fig. 2 | Crystal structure of BCOR^{N1607}/PCGF1^{RAWUL} dimer in complex with KDM2B^{LRRs}. **A** Structure of BCOR^{N1607}/PCGF1^{RAWUL}/KDM2B^{LRRs} heterotrimer is presented as cartoon. BCOR^{N1607}, PCGF1^{RAWUL} and KDM2B^{LRRs} are colored as magenta, yellow and blue, respectively. Residues for BCOR^{N1607} interacting with KDM2B^{LRRs} are shown as stick. **B** Binding affinity between BCOR$^{ANK\text{-}linker\text{-}PUFD}$ (wild type or P1620A/P1621A mutant)/PCGF1^{RAWUL} and KDM2B$^{F\text{-}box\text{-}LRRs}$ (wild type or W1143A mutant)/SKP1 was measured using ITC. The K_d values are shown as mean ± SD for triplicate experiments. **C** Sequence alignment of BCOR^{linker} among species from zebrafish to human. NPPGP motif on linker of BCOR is boxed with magenta dash.

Structures of BCOR/PCGF1/KDM2B/SKP1 tetramer constructed by integrative approaches

The affinity measurement data presented above demonstrates that NPPGP motif, Poly-D/E^{2nd} and Poly-D/E^{3rd} together are involved in BCOR binding to KDM2B (Fig. 1D). However, in the crystal structure, interactions between these Poly-D/E regions and KDM2B were not observed (Fig. 2A). One possible explanation is that this interaction may be disturbed during the crystallization process. To better understand the mechanism on how BCOR can be recruited by KDM2B, structure models of BCOR^{N1607} /PCGF1^{RAWUL}/KDM2B$^{F\text{-}box\text{-}LRRs}$/SKP1 and BCOR$^{ANK\text{-}linker\text{-}PUFD}$/PCGF1^{RAWUL}/KDM2B$^{F\text{-}box\text{-}LRRs}$/SKP1 were constructed using integrative approaches, including Small Angle X-ray Scattering (SAXS), molecular docking and cross-linking mass spectrometry (XL-MS).

To obtain distance information between domains of BCOR$^{ANK\text{-}linker\text{-}PUFD}$/ PCGF1^{RAWUL}dimer and KDM2B$^{F\text{-}box\text{-}LRRs}$/SKP1 dimer in the tetramer, the complex was subjected to crosslinking, followed by mass spectrometry analysis. Crosslinking analysis showed that LRRs of KDM2B were extensively cross-linked with RAWUL domain of PCGF1 by crosslinker BS3 (Fig. 3A, Supplementary Table 1 and 2), and ANK domain of BCOR was significantly cross-linked with SKP1 by crosslinker EDC (Fig. 3A, Supplementary Table 3). These results suggest that, in the complex of BCOR$^{ANK\text{-}linker\text{-}PUFD}$/PCGF1^{RAWUL}/KDM2B$^{F\text{-}box\text{-}LRRs}$/SKP1, BCOR^{PUFD}/PCGF1^{RAWUL} and KDM2B^{LRRs} are in close proximity, and ANK domain of BCOR is close to SKP1.

To construct the structure of BCOR^{N1607}/PCGF1^{RAWUL}/KDM2B$^{F\text{-}box\text{-}LRRs}$/SKP1, we collected SAXS data for the complex (Supplementary Table 4, Supplementary Fig. 1A, B). BCOR^{PUFD} (1634–1746)/PCGF1^{RAWUL} was docked onto KDM2B$^{F\text{-}box\text{-}LRRs}$/SKP1 with SAXS profile using software FoXSDock, then section of N1619-D1625 from BCOR linker was generated based on crystal structure of BCOR^{N1607}/PCGF1^{RAWUL}/KDM2B^{LRRs} heterotrimer, and finally residues E1607-A1618 and Q1626-S1633 from linker of BCOR were built using software ModLoop (Fig. 3B). The theoretical profile calculated from the derived model of BCOR^{N1607} /PCGF1^{RAWUL}/KDM2B$^{F\text{-}box\text{-}LRRs}$/SKP1 is in excellent agreement with the experimental SAXS profile, with a $\chi 2$ value of 1.04 (Fig. 3C). Additionally, the BCOR^{N1607} /PCGF1^{RAWUL}/KDM2B$^{F\text{-}box\text{-}LRRs}$/SKP1 model agrees well with the ab initio envelope (Fig. 3B).

To construct the structure of BCOR$^{ANK\text{-}linker\text{-}PUFD}$/PCGF1^{RAWUL}/KDM2B$^{F\text{-}box\text{-}LRRs}$/SKP1, ANK domain of BCOR predicted by AlphaFold2 was docked onto the complex of BCOR^{1607}/PCGF1^{RAWUL}/KDM2B$^{F\text{-}box\text{-}LRRs}$/SKP1, together with SAXS profile (Supplementary table 4, Supplementary Fig. 1C, D) and distance constrains based on EDC crosslinking data using software FoXSDock. The linker of BCOR was further completed with software ModLoop (Fig. 3D). The theoretical profile calculated from the derived model of BCOR$^{ANK\text{-}linker\text{-}PUFD}$/PCGF1^{RAWUL}/KDM2B$^{F\text{-}box\text{-}LRRs}$/SKP1 is in agreement with the experimental SAXS profile, with a $\chi 2$ value of 1.73 (Fig. 3E). This model also fits well with the ab initio envelope (Fig. 3D).

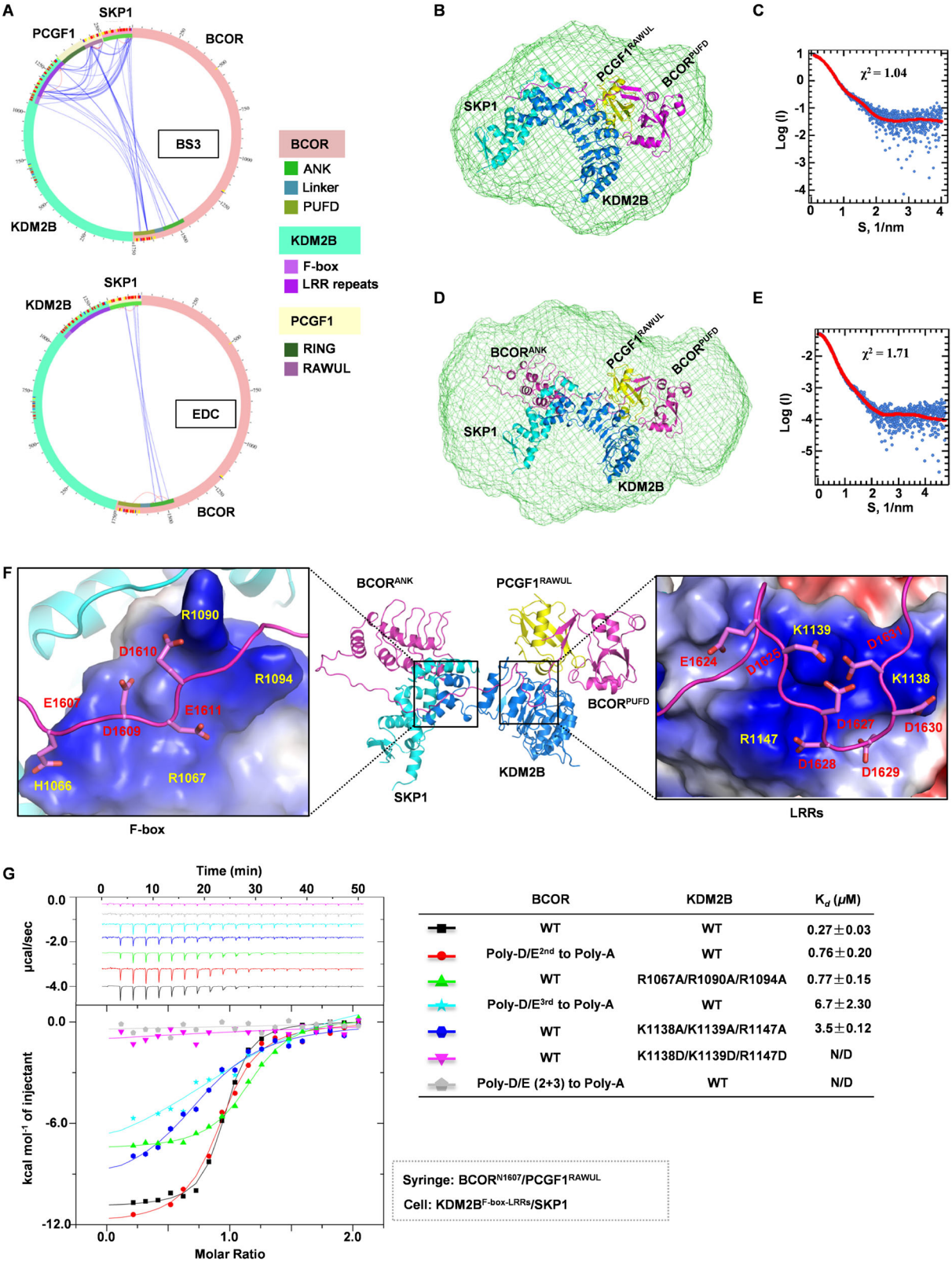

BCOR	KDM2B	K_d (μM)
WT	WT	0.27±0.03
Poly-D/E^{2nd} to Poly-A	WT	0.76±0.20
WT	R1067A/R1090A/R1094A	0.77±0.15
Poly-D/E^{3rd} to Poly-A	WT	6.7±2.30
WT	K1138A/K1139A/R1147A	3.5±0.12
WT	K1138D/K1139D/R1147D	N/D
Poly-D/E (2+3) to Poly-A	WT	N/D

Molecular mechanism of Poly-D/E regions of BCOR binding with KDM2B

In the modeled structure of BCOR$^{ANK\text{-}linker\text{-}PUFD}$/PCGF1^{RAWUL}/KDM2B$^{F\text{-}box\text{-}LRRs}$/SKP1 tetramer, we not only fit the NPPGP motif of BCOR as that in the crystal structure, but also obtain insights into the interaction of Poly-D/E regions on linker of BCOR. The Poly-D/E^{1st} (1591–1593) does not interact with KDM2B/SKP1 dimer, which is consistent with our affinity measurement that the Poly-D/E^{1st} does not contribute to the binding (Fig. 1D). On the other hand, the Poly-D/E^{2nd} (1607–1611) can form salt bridges with H1066, R1067, R1090 and R1094 from the F-box of KDM2B (Fig. 3F). These interactions were then confirmed by mutagenesis analysis that, the affinity of BCOR^{N1607}/PCGF1^{RAWUL} binding to KDM2B$^{F\text{-}box\text{-}LRRs}$/SKP1 was reduced

Fig. 3 | Structural models of BCOR/PCGF1/KDM2B/SKP1 tetramer. A A Circular plot illustrating the XL-MS analysis of the BCOR$^{ANK\text{-}linker\text{-}PUFD}$/PCGF1^{RAWUL}/KDM2B$^{F\text{-}box\text{-}LRRs}$/SKP1 complex cross-linked by crosslinker BS3 or EDC. **B** The structure model of BCOR^{N1607}/PCGF1^{RAWUL}/KDM2B$^{F\text{-}box\text{-}LRRs}$/SKP1 is overlaid with the ab initio structure envelope. The structure of BCOR^{N1607}/PCGF1^{RAWUL}/KDM2B$^{F\text{-}box\text{-}LRRs}$/SKP1 is modeled using FoXSDock and ModLoop. The ab initio envelope is determined by program GASBOR and averaged by DAMAVER. **C** Experimental SAXS profile overlaid with the theoretical profile calculated from modeled structure of BCOR^{N1607}/PCGF1^{RAWUL}/KDM2B$^{F\text{-}box\text{-}LRRs}$/SKP1. **D** The structure model of BCOR$^{ANK\text{-}linker\text{-}PUFD}$/PCGF1^{RAWUL}/KDM2B$^{F\text{-}box\text{-}LRRs}$/SKP1 is overlaid with the ab initio structure. The structure of BCOR$^{ANK\text{-}linker\text{-}PUFD}$/PCGF1^{RAWUL}/KDM2B$^{F\text{-}box\text{-}LRRs}$/SKP1 is modeled using FoXSDock and ModLoop. The ab initio envelope is determined by program GASBOR and averaged by DAMAVER. **E** Experimental SAXS profile overlaid with the theoretical profile calculated from modeled structure of BCOR$^{ANK\text{-}linker\text{-}PUFD}$/PCGF1^{RAWUL}/KDM2B$^{F\text{-}box\text{-}LRRs}$/SKP1. **F** Details for Poly-D/E^{2nd} and Poly-D/E^{3rd} on linker of BCOR interacting with positive patches on F-box and LRRs of KDM2B, respectively. BCOR, PCGF1 and SKP1 are shown cartoon, and colored as magenta, yellow and cyan, respectively; KDM2B is shown as blue cartoon or electrostatic surface. **G** Binding affinity between BCOR^{N1607} (wild type or mutation on Poly-D/E)/PCGF1^{RAWUL} and KDM2B$^{F\text{-}box\text{-}LRRs}$ (wild type or mutation on positive patch)/SKP1 was measured using ITC. N/D: Cannot be determined. The K_d values are shown as mean ± SD for triplicate experiments.

>2.5 fold, when D/E on Poly-D/E^{2nd} (1607–1611) were mutated to Ala, or R1067/R1090/R1094 from the F-box of KDM2B were mutated to Ala (Fig. 3G). The Poly-D/E^{3rd} (1624–1631) was predicted to form electrostatic interactions with K1138/K1139/R1147 from the second LRR of KDM2B (Fig. 3F). The binding site of Poly-D/E^{3rd} (1624–1631) was further confirmed by our findings that, the affinity of BCOR^{N1607} /PCGF1^{RAWUL} binding to KDM2B$^{F\text{-}box\text{-}LRRs}$/SKP1 was significantly reduced (>12 fold), when D/E on Poly-D/E^{3rd} (1624–1631) were mutated to Ala, or K1138/K1139/R1147 from KDM2B were mutated to Ala, and was almost abolished by mutating K1138/K1139/R1147 from KDM2B to Asp (Fig. 3G). Moreover, by mutating D/E residues on both Poly-D/E^{2nd} (1607–1611) and Poly–D/E^{3rd} (1624–1631) to Ala, interactions between BCOR^{N1607} /PCGF1^{RAWUL} and KDM2B$^{F\text{-}box\text{-}LRRs}$/SKP1 cannot be detected by ITC experiments (Fig. 3G). Our results further confirmed that electrostatic interactions mediated by Poly-D/E^{2nd} (1607–1611) and Poly-D/E^{3rd} (1624–1631) from linker of BCOR and positive patches on F-box and LRR repeats from KDM2B are indispensable for KDM2B recruiting BCOR-PRC1.1. Thus, within this BCOR$^{ANK\text{-}linker\text{-}PUFD}$/PCGF1^{RAWUL}/KDM2B$^{F\text{-}box\text{-}LRRs}$/SKP1 tetramer model, we observed extensive interactions contributed by Poly-D/E regions and NPPGP motif. The dependence of the Poly-D/E regions of linker for BCOR tethering enzymatic core with KDM2B is distinguished from the homologous BCORL1, in which PUFD domain alone is sufficient to mediate BCORL1-PRC1.1 assembly[28,33].

The binding between KDM2B and BCOR/PCGF1 was weakened by magnesium or calcium ions

Above analysis clearly shows that electrostatic interactions attributed by Poly-D/E^{2nd} (1607–1611) and Poly-D/E^{3rd} (1624–1631) are indispensable for BCOR binding to KDM2B. Intriguingly, strong interaction between Poly-D/E^{3rd} (1624–1631) and KDM2B^{LRRs} was not observed in the crystal structure of BCOR^{N1607}/PCGF1^{RAWUL}/KDM2B^{LRRs} heterotrimer. We noticed that the crystallization buffer contains 100 mM magnesium acetate. We hypothesized that Mg^{2+} may disrupt BCOR association with KDM2B by neutralizing Poly-D/E^{2nd} (1607–1611) and Poly-D/E^{3rd} (1624–1631). To test this notion, we determined the binding between BCOR^{N1607} /PCGF1^{RAWUL} dimer and KDM2B$^{F\text{-}box\text{-}LRRs}$/SKP1 dimer or KDM2B^{LRRs} in the presence of magnesium chloride. Indeed, BCOR^{N1607} /PCGF1^{RAWUL} dimer binding to KDM2B$^{F\text{-}box\text{-}LRRs}$/SKP1 dimer or KDM2B^{LRRs} was impaired by magnesium chloride in a concentration dependent manner (Supplementary Fig. 2A, B). To further verify whether Mg^{2+} can impair BCOR binding to KDM2B under cellular condition, Co-IP experiments were performed to analyze the interaction of exogenous Flag-tagged KDM2B with endogenous BCOR-PRC1.1 subunits in the presence of magnesium ion. As shown in Fig. 4A, B, binding affinity of KDM2B and BCOR/PCGF1 was significantly reduced in the presence of Mg^{2+} in IP buffer with concentration >200 μM.

It has been well demonstrated that calcium (Ca^{2+}) is one of the most important second messengers, in some instances specifically functioning in the nucleus, that regulate a variety of cellular functions such as senescence, cell death, proliferation[36–38].It is interesting to test whether KDM2B recruiting BCOR can be regulated by Ca^{2+}, when PRC1.1 complex serving as a transcription regulator. To this end, ITC and biolayer interferometry (BLI) were used to determine the interaction between BCOR$^{ANK\text{-}linker\text{-}PUFD}$/PCGF1^{RAWUL}dimer and KDM2B$^{F\text{-}box\text{-}LRRs}$/SKP1 dimer in the presence of Ca^{2+}. ITC experiments showed the binding affinity of BCOR$^{ANK\text{-}linker\text{-}PUFD}$/PCGF1^{RAWUL} to KDM2B$^{F\text{-}box\text{-}LRRs}$/SKP1 was significantly reduced with increased concentration of Ca^{2+}, indicating that this interaction is inhibited by Ca^{2+} (Supplementary Fig. 2C). Meanwhile, BLI assay also showed that Ca^{2+} can inhibit this interaction in a concentration dependent manner (Supplementary Fig. 2D). IP assay also showed that the interaction was impaired for exogenous Flag-tagged KDM2B and endogenous BCOR-PRC1.1 subunits, in the presence of calcium ions with concentration >25 μM (Fig. 4C, D). As a highly localized messenger, the concentration of Ca^{2+} can reaches over 100 μM near the mouth of ion channels upon stimulation[39]. Thus, these results suggest that KDM2B association with the core of BCOR-PRC1.1 can be weakened by calcium at increased physiological concentration.

Calcium ion induces liquid-liquid phase separation of BCOR$^{ANK\text{-}linker\text{-}PUFD}$/PCGF1^{RAWUL} heterodimer

Our structural studies and affinity determination have clearly identified that Poly-D/E^{2nd} (1607–1611) and Poly-D/E^{3rd} (1624–1631) on BCOR are critical for BCOR/PCGF1 associating with KDM2B (Fig. 3F, G). As expected, confocal microscopy showed that co-localization was substantially reduced for over-expressed BCOR-mCherry and KDM2B-EGFP, upon mutating Poly-D/E^{2nd} and Poly-D/E^{3rd} to Poly-A, without over-expressed PCGF1 (Fig. 5A). Interestingly, with the presence of over-expressed PCGF1, robust co-localization into punctate structures can be observed for KDM2B, PCGF1 and mutated BCOR (Poly-D/E^{2nd} and Poly-D/E^{3rd} to Poly-A) (Fig. 5B). This led us to speculate that the co-localization of KDM2B with PCGF1 and mutated BCOR (Poly-D/E^{2nd} and Poly-D/E^{3rd} to Poly-A) may be maintained by liquid-liquid phase separation (LLPS) mechanism, which was mediated by multivalent weak interactions. To test this, we explored the LLPS property of Poly-D/E mutated BCOR$^{ANK\text{-}linker\text{-}PUFD}$ /PCGF1^{RAWUL} dimer. As shown in Supplementary Fig. 3A, just mutating Poly-D/E^{3rd} to Poly-A, BCOR$^{ANK\text{-}linker\text{-}PUFD}$ mutant /PCGF1^{RAWUL} dimer, but not the monomeric BCOR$^{ANK\text{-}linker\text{-}PUFD}$ mutant, formed phase separation in protein concentration dependent manners (Supplementary Fig. 3B). Additionally, the mutated BCOR$^{ANK\text{-}linker\text{-}PUFD}$/PCGF1^{RAWUL} also formed condensates in live HeLa cells (Fig. 5C).

Then, we tested whether Ca^{2+} could induce phase separation of BCOR$^{ANK\text{-}linker\text{-}PUFD}$/PCGF1^{RAWUL} by neutralizing negative charged Poly-D/E region. Indeed, BCOR$^{ANK\text{-}linker\text{-}PUFD}$/PCGF1^{RAWUL} formed phase separation in $CaCl_2$ and NaCl concentration dependent manners (Fig. 5D,). To investigate the liquid-like nature of BCOR$^{ANK\text{-}linker\text{-}PUFD}$/PCGF1^{RAWUL} condensates, we performed fusion events observation and fluorescence recovery after photobleaching (FRAP) experiments. Rapid fusion of BCOR$^{ANK\text{-}linker\text{-}PUFD}$/PCGF1^{RAWUL} condensates can be observed under time lapse microscopy (Fig. 5E). In addition, rapid recovery of fluorescence in BCOR$^{ANK\text{-}linker\text{-}PUFD}$/PCGF1^{RAWUL} condensates was observed after photo-bleaching (Fig. 5F). Evidently, liquid-like property of BCOR$^{ANK\text{-}linker\text{-}PUFD}$/PCGF1^{RAWUL} condensate is induced by $CaCl_2$. While Mg^{2+} is the most abundant bivalent cation in cell, we also performed LLPS experiments in the presence of $MgCl_2$. The ability of $MgCl_2$, at concentration as high as 25 mM, to induce LLPS of BCOR$^{ANK\text{-}linker\text{-}PUFD}$/PCGF1^{RAWUL} (at 100 μM), is comparable with that of $CaCl_2$ at concentration of 1 mM (Supplementary Fig. 4).

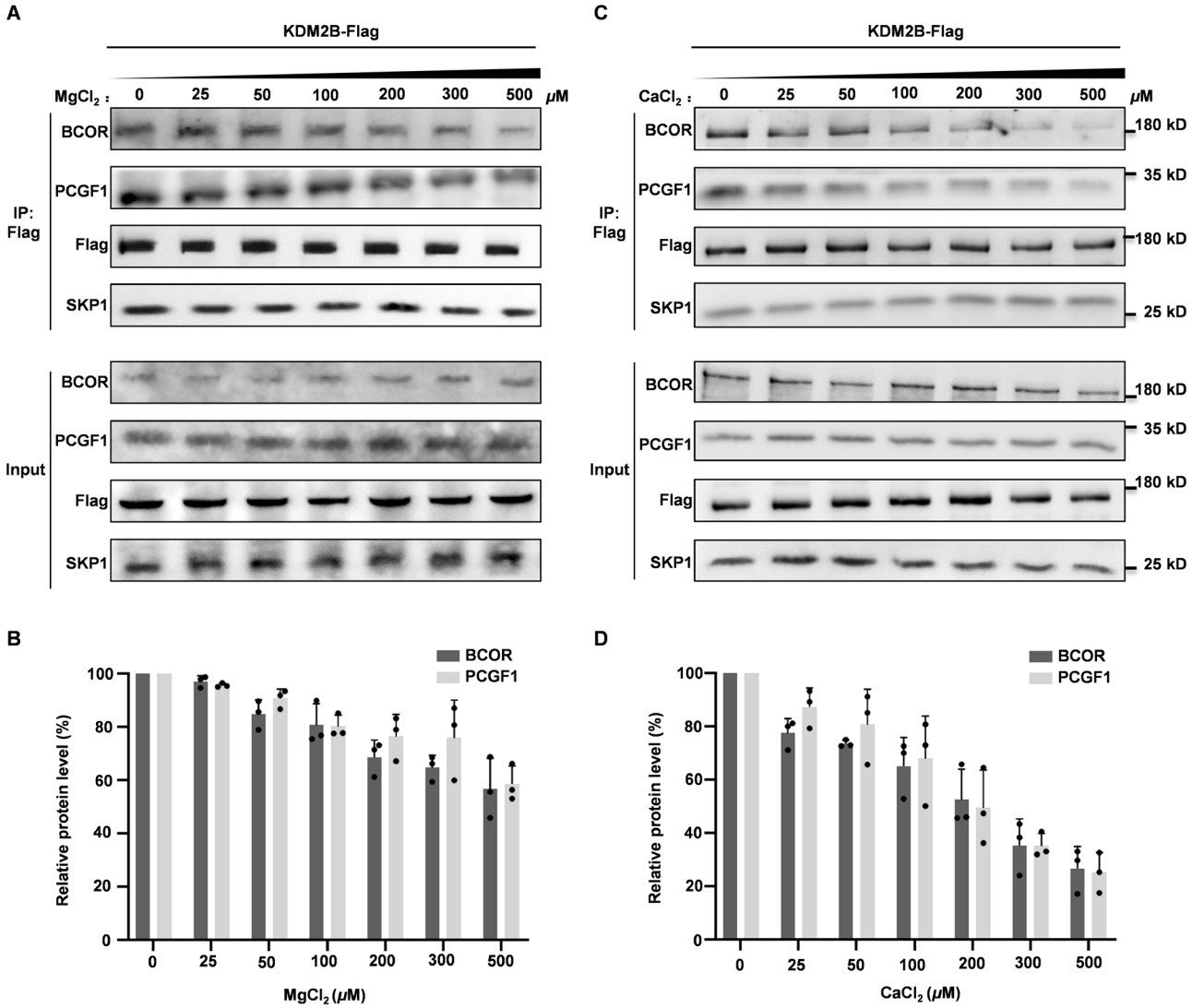

Fig. 4 | Effect of magnesium ion or calcium ion on BCOR binding to KDM2B. **A** Analyzing the effect of magnesium ion on over-expressed KDM2B-Flag binding to endogenous BCOR, PCGF1 and SKP1 using Co-IP assay. The western-blotting data is representative of three independent experiments. **B** Relative level of BCOR or PCGF1 protein co-purified with KDM2B-Flag as shown in (**A**). Data are represented as mean ± SD for triplicate experiments. **C** Analyzing the effect of calcium on over-expressed KDM2B-Flag binding to endogenous BCOR, PCGF1 and SKP1 using Co-IP assay. The western-blotting data is representative of three independent experiments. **D** Relative level of BCOR or PCGF1 protein co-purified with KDM2B-Flag as shown in (**C**). Data are represented as mean ± SD for triplicate experiments. Expressing plasmid for KDM2B-Flag was transfected into HEK293T cells. Co-IP was performed with anti-Flag magnetic beads, after 48 h transfection. $MgCl_2$ or $CaCl_2$ at indicated concentration is supplemented to IP buffer.

It is interesting to uncover which sequence motif directly contributes to the condensation of $BCOR^{ANK\text{-}linker\text{-}PUFD}$/$PCGF1^{RAWUL}$, besides the Ca^{2+}. π-interaction was suggested as one of the common drivers for LLPS formation[40]. There are five aromatic residues on the linker of BCOR, including W1598, F1600, Y1601, Y1614 and Y1633 (Fig. 1A), and named as "WFY". After mutating these residues to Ala, $CaCl_2$ failed to induce LLPS of $BCOR^{ANK\text{-}linker\text{-}PUFD}$/$PCGF1^{RAWUL}$ (Supplementary Fig. 5A). Consistently, these aromatic residues were required for LLPS of $BCOR^{ANK\text{-}linker\text{-}PUFD}$ (Poly-D/E^{3rd} to Poly-A)/$PCGF1^{RAWUL}$, in solution or in cells (Fig. 5C and Supplementary Fig. 5B).

Given the fact that $BCOR^{ANK\text{-}linker\text{-}PUFD}$/$PCGF1^{RAWUL}$ could not phase separate spontaneously in live Hela cells (Fig. 5C), physiologically relevant concentration of Mg^{2+} is insufficient to induce LLPS of $BCOR^{ANK\text{-}linker\text{-}PUFD}$/$PCGF1^{RAWUL}$. We then tested whether phase separation of $BCOR^{ANK\text{-}linker\text{-}PUFD}$/$PCGF1^{RAWUL}$ in live cell could be induced by cellular calcium. As shown in Fig. 5H, after calcium influx is induced by 10 μM ionomycin, liquid-like droplet of $BCOR^{ANK\text{-}linker\text{-}PUFD}$/$PCGF1^{RAWUL}$ can be observed in live HeLa cells. Moreover, the ionomycin induced LLPS can be reversed by treatment with 10 μM calcium-chelator BAPTA-AM (Fig. 5H).

Taken together, these results demonstrated that, via neutralizing the negatively charged Poly-D/E region on BCOR, Ca^{2+} or Mg^{2+} can induce the liquid-liquid phase separation of $BCOR^{ANK\text{-}linker\text{-}PUFD}$/$PCGF1^{RAWUL}$ in solution. More importantly, elevated Ca^{2+} concentration is required to trigger the phase separation of $BCOR^{ANK\text{-}linker\text{-}PUFD}$/$PCGF1^{RAWUL}$ under cellular condition.

Co-condensation of enzymatic core of BCOR–PRC1.1 with KDM2B via Ca^{2+} stimulated LLPS mechanism

Given that KDM2B tightly associates with the linker on BCOR, here, we test whether $KDM2B^{F\text{-}box\text{-}LRRs}$/SKP1 can influence Ca^{2+} induced LLPS of $BCOR^{ANK\text{-}linker\text{-}PUFD}$/$PCGF1^{RAWUL}$. We performed LLPS experiments in the presence of $KDM2B^{F\text{-}box\text{-}LRRs}$/SKP1 dimer. Under microscopy observation, we found that $CaCl_2$ induced LLPS of $BCOR^{ANK\text{-}linker\text{-}PUFD}$/$PCGF1^{RAWUL}$ was significantly decreased, with increasing concentration of $KDM2B^{F\text{-}box\text{-}LRRs}$/SKP1 dimer (Fig. 6A). After mutating K1138/K1139/R1147 on KDM2B to

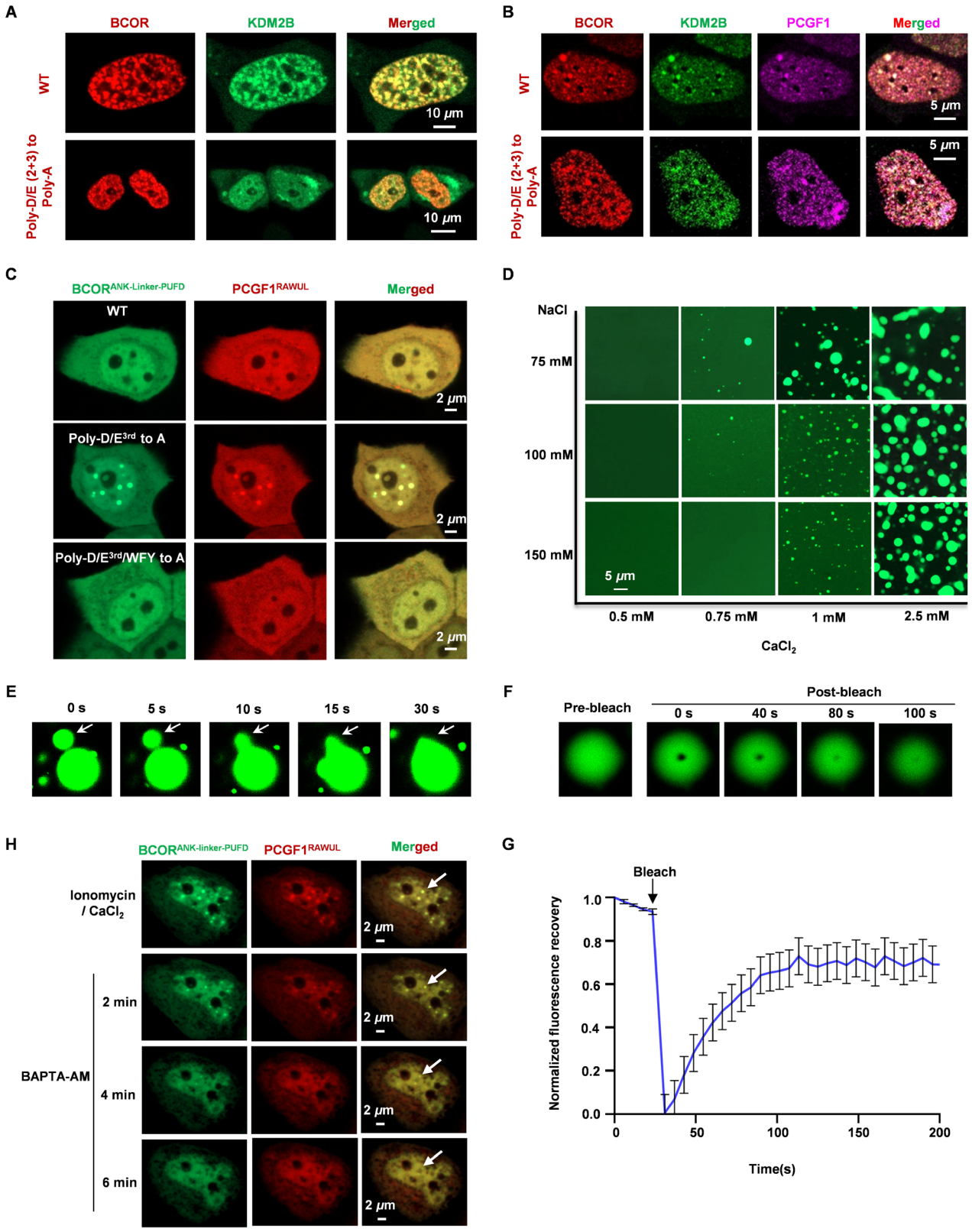

Asp, KDM2B$^{F\text{-box-LRRs}}$ (K1138D/K1139D/R1147D mutant)/SKP1 dimer showed reduced capacity to impair Ca^{2+} induced LLPS of BCOR$^{ANK\text{-linker-PUFD}}$/PCGF1^{RAWUL} (Fig. 6B), most likely resulting from its decreased binding capacity to BCOR$^{ANK\text{-linker-PUFD}}$/PCGF1^{RAWUL}. These suggest that, by binding to BCOR$^{ANK\text{-linker-PUFD}}$/PCGF1^{RAWUL}, KDM2B$^{F\text{-box-LRRs}}$/SKP1 competitively inhibits Ca^{2+} induced LLPS of BCOR$^{ANK\text{-linker-PUFD}}$/PCGF1^{RAWUL}.

As shown in Fig. 6A, with KDM2B$^{F\text{-box-LRRs}}$/SKP1 dimer at <25 μM, robust Ca^{2+} (5 mM) stimulated condensates of BCOR$^{ANK\text{-linker-PUFD}}$/PCGF1^{RAWUL} (100 μM) can be observed under microscopy observation. Then, we performed co-localization analysis for KDM2B$^{F\text{-box-LRRs}}$/SKP1-mCherry (10 μM) and LLPS droplets of EGFP-BCOR$^{ANK\text{-linker-PUFD}}$/PCGF1^{RAWUL} (100 μM) induced by Ca^{2+}. Surprisingly, we found that

Fig. 5 | Liquid-liquid phase separation of BCOR$^{ANK\text{-}linker\text{-}PUFD}$/PCGF1^{RAWUL} hetero-dimer. A Co-localization analysis of BCOR-mCherry with KDM2B-EGFP in live HeLa cells. **B** Co-localization analysis of BCOR-mCherry, PCGF1-ECFP and KDM2B-EGFP in live HeLa cells. **C** Observation of condensates for BCOR$^{ANK\text{-}linker\text{-}PUFD}$ (wild type or mutant)/PCGF1^{RAWUL} in HeLa cells. WFY indicates the 5 aromatic residues on linker of BCOR, including W1598, F1600, Y1601, Y1614 and Y1633. **D** Effect of $CaCl_2$ and NaCl on the phase separation of BCOR$^{ANK\text{-}linker\text{-}PUFD}$/PCGF1^{RAWUL} hetero-dimer with concentration of 60 μM. **E** Representative fusion event of BCOR$^{ANK\text{-}linker\text{-}PUFD}$/PCGF1^{RAWUL} droplets. **F** In vitro FRAP analysis of the droplet of BCOR$^{ANK\text{-}linker\text{-}PUFD}$/PCGF1^{RAWUL}. **G** Normalized FRAP recovery curves for BCOR$^{ANK\text{-}linker\text{-}PUFD\text{-}EGFP}$/PCGF1^{RAWUL} droplet in (**F**). Data are mean ± SEM at each time point and combined data from three independent repeats. **H** Plasmids expressing BCOR$^{ANK\text{-}Linker\text{-}PUFD}$ or PCGF1^{RAWUL} were co-transfected into HeLa cell. Before imaging for LLPS, cells were pretreated with 10 μM ionomycin and 5 mM $CaCl_2$ for 2 h. To observe the effect of calcium-chelator BAPTA-AM on the ionomycin induced LLPS, culture containing 10 μM ionomycin and 5 mM $CaCl_2$ was discarded, the cell was washed with PBS, then culture containing 10 μM BAPTA-AM was added to the cell.

KDM2B$^{F\text{-}box\text{-}LRRs}$/SKP1 can be partitioned together with BCOR$^{ANK\text{-}linker\text{-}PUFD}$/PCGF1^{RAWUL}, when KDM2B$^{F\text{-}box\text{-}LRRs}$/SKP1-mCherry (10 μM) was mixed with EGFP-BCOR$^{ANK\text{-}linker\text{-}PUFD}$/PCGF1^{RAWUL} (100 μM) before treatment with 5 mM $CaCl_2$ (Fig. 6C). When BCOR$^{ANK\text{-}linker\text{-}PUFD}$/PCGF1^{RAWUL} (100 μM) was pretreated with 5 mM $CaCl_2$ before mixing with KDM2B$^{F\text{-}box\text{-}LRRs}$/SKP1 (10 μM), KDM2B$^{F\text{-}box\text{-}LRRs}$/SKP1 was enriched on the periphery of BCOR$^{ANK\text{-}linker\text{-}PUFD}$/PCGF1^{RAWUL} condensates (Fig. 6D). With time lapse microscopy, we observed that KDM2B$^{F\text{-}box\text{-}LRRs}$/SKP1 diffused toward inner side of the condensates (Fig. 6D). These results suggest that Ca^{2+} induces co-segregation of BCOR$^{ANK\text{-}linker\text{-}PUFD}$/PCGF1^{RAWUL} with KDM2B/SKP1.

To further validate that Ca^{2+} can induce con-condensation of BCOR-PRC1.1 with KDM2B, we performed LLPS experiments for BCOR$^{ANK\text{-}linker\text{-}PUFD}$/PCGF1$^{\Delta N35}$/Ring1B. As shown in Supplementary Fig. 6, BCOR$^{ANK\text{-}linker\text{-}PUFD}$/PCGF1$^{\Delta N35}$/Ring1B formed LLPS dependent on the presence of $CaCl_2$. Co-localization analysis also showed that KDM2B$^{F\text{-}box\text{-}LRRs}$/SKP1 could localize to Ca^{2+} induced droplets of BCOR$^{ANK\text{-}linker\text{-}PUFD}$/PCGF1$^{\Delta N35}$/Ring1B (Fig. 6E). We have demonstrated that mutating Poly-D/E to Poly-A mimics Ca^{2+} induced LLPS of BCOR$^{ANK\text{-}linker\text{-}PUFD}$/PCGF1^{RAWUL}. To further confirm that Ca^{2+} induced LLPS can modulate co-condensation of core subunits of BCOR-PRC1.1 with KDM2B in cell, we determined whether the co-localization of KDM2B together with PCGF1 and mutated BCOR (Poly-D/E^{2nd} and Poly-D/E^{3rd} to Poly-A) was dependent on LLPS of BCOR$^{ANK\text{-}linker\text{-}PUFD}$/PCGF1^{RAWUL}. To this end, aromatic residues on the linker of BCOR, which is critical for the LLPS of BCOR$^{ANK\text{-}linker\text{-}PUFD}$/PCGF1^{RAWUL} induced by Ca^{2+} or Poly-D/E mutation, were mutated to Ala. As shown in Fig. 6F, by mutating these residues, KDM2B could not condensate with PCGF1/ BCOR (Poly-D/E^{2nd} and Poly-D/E^{3rd} to Poly-A). Given the fact that aromatic residues on linker of BCOR were dispensable for the affinity of BCOR/PCGF1 binding to KDM2B (Fig. 6G, and Supplementary Fig. 7) and the core subunits of BCOR-PRC1.1 binding to chromatin (Supplementary Fig. 8), we concluded that co-condensation of BCOR (Poly-D/E^{2nd} and Poly-D/E^{3rd} to Poly-A) mutant, PCGF1 and KDM2B, was maintained through LLPS mechanism. Furthermore, heterochromatin puncta were overlapped well with condensates of mutated BCOR (Poly-D/E^{2nd} and Poly-D/E^{3rd} to Poly-A) together with PCGF1 and KDM2B (Fig. 6F). Interestingly, when mutating aromatic residues on linker of BCOR (BCOR$^{WFY/A}$) thereby disrupting Ca^{2+} induced LLPS of BCOR$^{ANK\text{-}linker\text{-}PUFD}$/PCGF1^{RAWUL}, the expression of two well-demonstrated PRC1.1 targets *HOXB7*[25] and *HOXA9*[41] was significantly increased (Fig. 6H, and Supplementary Fig. 9). This suggests that Ca^{2+} induced LLPS of BCOR$^{ANK\text{-}linker\text{-}PUFD}$/PCGF1^{RAWUL} is functionally relevant for PRC1.1. Taken together, these results indicate that Ca^{2+} may modulate condensation of BCOR-PRC1.1 on KDM2B target loci, through neutralizing the Poly-D/E region on linker of BCOR, which may promote gene silencing and compaction of chromatin on target loci.

Discussion

Despite the well-established fact that KDM2B recruiting PRC1.1 to CpG islands is essential for repressing expression of development regulator genes[20,27,28], there are still fundamental gaps in understanding how to regulate PRC1.1 recruitment to KDM2B occupied CpG-rich promoters. In this study, we clarified the molecular mechanism on BCOR$^{ANK\text{-}linker\text{-}PUFD}$/PCGF1^{RAWUL} interaction with KDM2B$^{F\text{-}box\text{-}LRRs}$/SKP1 through integrative structural approach. With this, we unveiled that the enzymatic core of BCOR-PRC1.1 can be loosened from KDM2B in the presence Ca^{2+}. Interestingly, our results also showed that Ca^{2+} could induce condensation of BCOR-PRC1.1 together with KDM2B on heterochromatin puncta through liquid-liquid phase separation.

Previous studies have identified the importance of the linker region of BCOR located between ANK repeats and PUFD domain in the process of KDM2B recruiting BCOR-PRC1.1 to targeted loci[22]. The mechanistic details on the linker region of BCOR binding to KDM2B remain elusive, due to the lack of structural information. In this study, we demonstrated that Poly-D/E^{2nd} (1607–1611) and Poly-D/E^{3rd} (1624–1631) on the linker of BCOR form electrostatic interaction with positively charged patch on the F-box and LRRs of KDM2B. We proposed that BCOR interaction with KDM2B may be weakened via neutralizing the Poly-D/E regions by metal ion. As a universal second messenger, calcium (Ca^{2+}) signaling is involved in various cellular processes, including fertilization, stem cell identity, muscle contraction, secretion, synaptic transmission, memory, gene transcription and cell death[42–46]. Calcium can regulate gene transcription, often through binding to calmodulin, and stimulates translocation of transcription factor from cytosol to nucleus or exportation of epigenetic regulator from the nucleus[37,47,48]. However, the direct role of calcium on epigenetic regulator has not been demonstrated in previous studies. In this study, we found that calcium can act on epigenetic regulator BCOR-PRC1.1 by loosening BCOR/PCGF1 heterodimer from KDM2B/SKP1 heterodimer. Our results provide the first example that calcium directly regulates activity of epigenetic regulator.

In resting state, the cellular level of free Ca^{2+} is usually maintained at low concentration of ~100 nM[45,49]. In response to stimuli, Ca^{2+} is released from extracellular or intracellular stores, and the local concentration can reach over 100 μM (at the mouth of channels)[39]. With Co-IP experiment, we identified that BCOR/PCGF1 interaction with KDM2B was largely weakened in the presence of 100 μM Ca^{2+}. This may suggest that rapidly released Ca^{2+} may regulate the association of enzymatic core of BCOR-PRC1.1 with KDM2B.

In addition to calcium signaling, liquid-liquid phase separation has also been implicated in transcription control through regulating chromatin organization[50–52]. Polycomb proteins have been demonstrated to concentrate into membrane-less organelle called Polycomb body via phase separation mechanism[53–55]. Polycomb protein CBX2, a component of canonical PRC1, condensates CBX2-PRC1 together with nucleosome via LLPS driven by charged low-complexity disordered region (LCDR)[56]. Our work uncovers another phase separation driver of PRC1 complex. We find that BCOR/PCGF1 dimer, components of non-canonical BCOR-PRC1.1, forms phase separated condensates driven by Ca^{2+}. CpG reader KDM2B can be concentrated into Ca^{2+} induced BCOR/PCGF1 condensates. Thus, our work suggests that repression effect of BCOR-PRC1.1 on transcription would be amplified by Ca^{2+} via LLPS mechanism.

Our ITC experiments and Co-IP assays clearly showed that BCOR/PCGF1 interaction with KDM2B could also be weakened by Mg^{2+}. In additional, the LLPS of BCOR$^{ANK\text{-}linker\text{-}PUFD}$/PCGF1^{RAWUL} also can be induced by high concentration of Mg^{2+}. Unlike calcium, free magnesium is abundant in cellular, with concentration in the range of 203.68 to 673.50 μM (in platelets)[57]. This suggests that Ca^{2+} may cooperate with Mg^{2+} to reduce the affinity of enzymatic core of BCOR-PRC1.1 with KDM2B, and to trigger the LLPS of BCOR$^{ANK\text{-}linker\text{-}PUFD}$/PCGF1^{RAWUL}.

BCORL1 is a homolog of BCOR. Previous study revealed that, PUFD domain of BCORL1 is sufficient to associate core subunits of PRC1.1 with

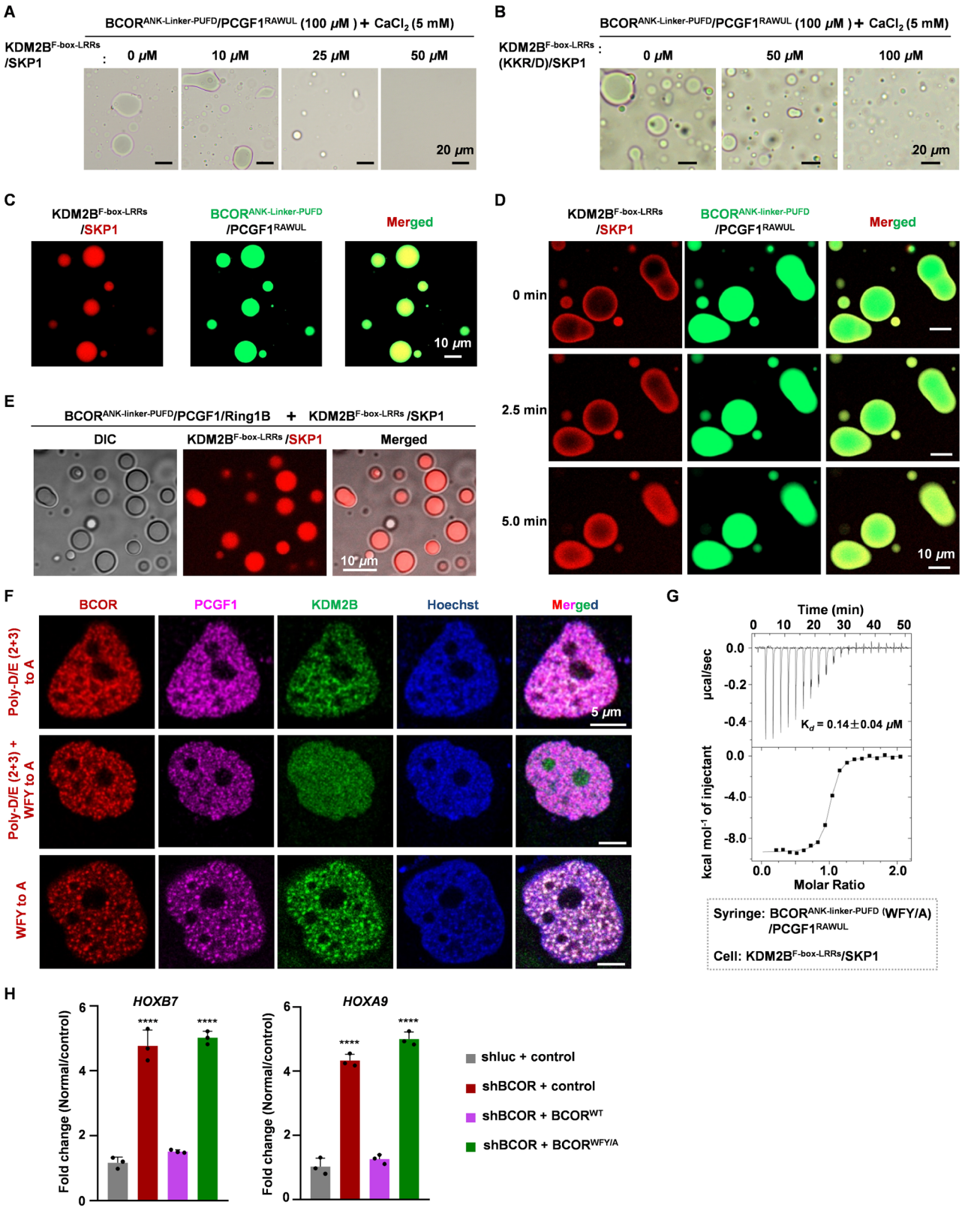

KDM2B, and E1664 is indispensable for this activity of BCORL1[32]. In BCOR, the Glu is substituted by L1705. The consequence of this substitution is that PUFD domain of BCOR is insufficient to associate core subunits of PRC1.1 with KDM2B. Whereas, the linker region is indispensable for BCOR to connect core subunits of PRC1.1 with KDM2B. Sequence alignment showed that, D/E is less enriched in linker of BCORL1 than that of BCOR (Supplementary Fig. 10). These analyses suggest that calcium regulation may be unique in the assembly of BCOR-PRC1.1 at CpG islands. Interestingly, sequence analysis shows that L1705 is only conserved in mammalian BCOR (Supplementary Fig. 10). In species from chicken to zebrafish, this L1705 is replaced by Glu, same as that in BCORL1, which may imply that the assembly of BCOR-PRC1.1 cannot be regulated by calcium in these

Fig. 6 | KDM2B co-segregates together with BCOR /PCGF1 in Ca^{2+} induced droplets. A, **B** Effects of $KDM2B^{F\text{-}box\text{-}LRRs}$/SKP1(**A**) or $KDM2B^{F\text{-}box\text{-}LRRs}$(KKR/D)/SKP1 (**B**) on condensates of $BCOR^{ANK\text{-}linker\text{-}PUFD}$/$PCGF1^{RAWUL}$. Before mixing with $KDM2B^{F\text{-}box\text{-}LRRs}$/SKP1 or $KDM2B^{F\text{-}box\text{-}LRRs}$(KKR/D)/SKP1, $BCOR^{ANK\text{-}linker\text{-}PUFD}$/$PCGF1^{RAWUL}$ (100 μM) was mixed with 5 mM $CaCl_2$ to stimulate droplets formation. **C, D** Co-localization analysis of $KDM2B^{F\text{-}box\text{-}LRRs}$/SKP1 and $BCOR^{ANK\text{-}linker\text{-}PUFD}$/$PCGF1^{RAWUL}$ in Ca^{2+} induced droplets. For (**C**), $KDM2B^{F\text{-}box\text{-}LRRs}$/SKP1-mCherry or $KDM2B^{F\text{-}box\text{-}LRRs}$(KKR/D)/SKP1-mCherry (10 μM) was mixed with GFP-$BCOR^{ANK\text{-}linker\text{-}PUFD}$/$PCGF1^{RAWUL}$ (100 μM), then 5 mM $CaCl_2$ was added to induce droplet formation. For (**D**), $BCOR^{ANK\text{-}linker\text{-}PUFD}$/$PCGF1^{RAWUL}$ (100 μM) was incubated with 5 mM $CaCl_2$ to stimulate droplets formation, then $KDM2B^{F\text{-}box\text{-}LRRs}$/SKP1-mCherry or $KDM2B^{F\text{-}box\text{-}LRRs}$(KKR/D)/SKP1-mCherry (10 μM) was added to the mixture immediately. $KDM2B^{F\text{-}box\text{-}LRRs}$(KKR/D) indicates that residues K1138, K1139 and R1147 on $KDM2B^{F\text{-}box\text{-}LRRs}$ were mutated to Asp. **E** Co-localization analysis of $KDM2B^{F\text{-}box\text{-}LRRs}$/SKP1-mCherry with $CaCl_2$ induced $BCOR^{ANK\text{-}linker\text{-}PUFD}$/$PCGF1^{\Delta N35}$/Ring1B droplets. $KDM2B^{F\text{-}box\text{-}LRRs}$/SKP1-mCherry (6 μM) was mixed with $BCOR^{ANK\text{-}linker\text{-}PUFD}$/$PCGF1^{\Delta N35}$/Ring1B (60 μM), then 5 mM $CaCl_2$ was added to induce droplet formation. **F** Co-localization analysis of BCOR-mCherry mutant, PCGF1-ECFP and KDM2B-EGFP in live HeLa cells. DNA was stained by Hoechst 33258 (Blue). **G** Binding affinity between $BCOR^{ANK\text{-}linker\text{-}PUFD}$ (WFY to A)/$PCGF1^{RAWUL}$ and $KDM2B^{F\text{-}box\text{-}LRRs}$/SKP1 was measured using ITC. The K_d values are shown as mean ± SD for triplicate experiments. **H** Effect of $BCOR^{WFY/A}$ mutant on the transcription of *HOXB7* and *HOXA9* in HEK293T cells. Empty vector was used as a negative control. shluc was used as control shRNA. ****$p < 0.0001$. Error bars represent standard deviation from 3 individual samples.

species. We speculate that the inhibitory effect of calcium on KDM2B recruiting BCOR-PRC1.1 to CpG islands is the consequence of evolution.

Previous studies showed that components of PRC1.1 are frequently up-regulated in acute myeloid leukemia (AML) patients[24]. In line with this finding, Leukemogenesis was suppressed by down-regulating PRC1.1 components including BCOR, PCGF1 and Ring1B[24,58]. In addition to AML cells, BCOR-PRC1.1 mediated H2A monoubiquitylation is critical for prostate cancer by repressing expression of a subset of androgen receptor target genes[25]. These imply that disrupting KDM2B recruitment of enzymatic core of BCOR-PRC1.1 is a potential strategy to treat leukemia and prostate cancer.

Taken together, the results presented here clearly showed that, by neutralizing Poly-D/E regions on BCOR, Ca^{2+} not only can reduce the affinity of KDM2B and enzymatic core of BCOR-PRC1.1, but also can condensate them into liquid-like droplet through liquid-liquid phase separation mechanism (Fig. 7). Via liquid-liquid phase separation, Ca^{2+} may effectively enhance the action of BCOR-PRC1.1 on target loci. Thus, our finding on Ca^{2+} induced liquid-liquid phase separation of BCOR/PCGF1, not only underpin the understanding how the behavior of BCOR-PRC1.1 is physiologically regulated, but also facilitate the development of potential strategy against cancers by modulating the action of BCOR-PRC1.1 on target loci.

Methods

Expression and purification

For bacterial expression, cDNA encoding truncations of BCOR, $KDM2B^{F\text{-}box\text{-}LRRs}$ (residues 1059–1336) and $KDM2B^{LRRs}$ (residues 1103–1336) were cloned into pET-28a with N-terminal hexa-histidine tag and TEV cleavage site; cDNA encoding $PCGF1^{RAWUL}$ (residues 150–255) and SKP1 were cloned into pET-21a without his-tag. $BCOR^{ANK\text{-}linker}$ (residues 1461-1635), BCOR/$PCGF1^{RAWUL}$ dimer, $KDM2B^{F\text{-}box\text{-}LRRs}$/SKP1 dimer and $KDM2B^{LRRs}$ (residues 1103–1336) were expressed in BL21 (DE3) cells. Cells were grown in LB medium at 37 °C until OD_{600} of 0.6 ~ 0.8, then expression was induced with 0.2 mM isopropyl-b-D-thiogalactoside (IPTG) for overnight at 16 °C. Cells were collected and re-suspected with lysis buffer (50 mM Tris pH 8.0, 300 mM NaCl, 10 mM imidazole, 1 mM PMSF, 5 mM β-mercaptoethanol and 5% glycerol). Proteins were purified using Ni^{2+} affinity chromatography. Truncations of BCOR and KDM2B were digested with TEV to remove the N-terminal his-tag. The proteins were further purified by ion exchange chromatography, and followed by gel filtration equilibrated against buffer containing 20 mM Tris pH 7.5, 150 mM NaCl and 0.5 mM TCEP. The $BCOR^{ANK\text{-}linker\text{-}PUFD}$ (Poly-D/E^{3rd} to Poly-A)/$PCGF1^{RAWUL}$ was purified by Ni^{2+} affinity chromatography and gel filtration with buffer containing 1 M NaCl.

Isothermal titration calorimetry (ITC)

ITC experiments were performed using a Microcal ITC200 instrument. Protein sample in syringe at concentration of 300 μM was titrated into protein sample in cell at concentration of 30 μM in 20 × 2 μL. All Protein samples were dissolved in 20 mM Tris pH7.5, 50 mM NaCl or 150 mM NaCl, 0.5 mM TCEP. Data was analyzed and the figure was prepared using Origin 7.

Co-immunoprecipitation (Co-IP)

HEK293T cells in 10 cm dish were cultured to 70%-80% density to conduct gene transfection. For the interaction identification via co-immunoprecipitation, the plasmid of BCOR-Flag (wild type or mutant) was co-transfected with PCGF1-Strep, KDM2B-HA and SKP1-Strep. Each plasmid of experiment group was transfected with 10 μg. Cells were collected after 48 h and lysed with lysis buffer (50 mM Tris pH7.4, 150 mM NaCl, 5% glycerol, 1% NP-40) with 1 mM protease inhibitor cocktail (Roche) and 1 mM PMSF at 4 °C for 30 min. Cell lysates were clarified by centrifugation at 4 °C for 30 min. Then the 20 μL anti-Flag magnetic beads, which was washed with IP buffer (50 mM Tris pH7.4, 150 mM NaCl, 5% glycerol) for 3 times, was added into the supernatant with 2 times the volume IP buffer and incubated at 4 °C overnight. The magnetic bead was washed with IP wash buffer (50 mM Tris pH 7.4, 150 mM NaCl, 5% glycerol, 0.1% NP-40) with 1 mM PMSF for 3 times. Finally, the magnetic bead was eluted by the IP wash buffer with 120 μL 3 x Flag peptide and 1 mM protease inhibitor cocktail (Roche) and 1 mM PMSF at 4 °C for 2 h. The eluent was then analyzed by western blot.

To verify the effect of magnesium or calcium ions on the binding of KDM2B to BCOR, the plasmid of KDM2B-Flag was transfected to HEK293F cells. The cells were counted every 24 h after transfection, and 15×10^6 cells per EP tube were collected after about 72 h of culture when the viability of the cells was about 80%. Cells were lysed with lysis buffer (50 mM Tris pH7.4, 150 mM NaCl, 5% glycerol, 1% NP-40) with 1 mM protease inhibitor cocktail (Roche) and 1 mM PMSF at 4 °C for 30 min. Cell lysates were clarified by centrifugation at 4 °C for 30 min. The supernatant was collected, divided into aliquots and added with different concentrations of calcium chloride. Then, Co-IP experiment was performed using anti-Flag magnetic beads with calcium chloride at indicated concentration.

Crystallization and structure determination

To obtain $BCOR^{N1607}$/$PCGF1^{RAWUL}$/$KDM2B^{LRRs}$ heterotrimer, $BCOR^{N1607}$/$PCGF1^{RAWUL}$ was mixed with $KDM2B^{LRRs}$ heterotrimer at mole ratio 1:1, and purified with gel filtration. For crystallization screening, $BCOR^{N1607}$/$PCGF1^{RAWUL}$/$KDM2B^{LRRs}$ was concentrated to 10 mg/mL and sitting drop vapor diffusion method was used by mixing protein with reservoir solution at volume ratio 1:1 at 20 °C. Crystals of $BCOR^{N1607}$/$PCGF1^{RAWUL}$/$KDM2B^{LRRs}$ heterotrimer were grown with reservoir solution containing 0.1 M magnesium acetate, 0.1 M sodium citrate pH 6.1, 4% w/v PEG5000 MME.

Crystals were cryoprotected in mother liquid with addition of 30% glycerol, prior to diffraction. Diffraction data was collected at Beam Line 19U1 (BL19U1)[59] of National center for Protein Science Shanghai and the Shanghai Synchrotron Radiation Facility. Diffraction data was processed with automatic data-processing system Aquarium, and scaled with Aimless[60]. Crystal structure was solved by molecule replacement with software Molrep[61] using crystal structures of $KDM2B^{LRRs}$ (PDB code 5JH5) and $BCOR^{PUFD}$/$PCGF1^{RAWUL}$ heterodimer (PDB code 4HPL) as starting model. Coot was used to complete the model building. Refinement of structure was conducted using Refmac5[62]. Data collection and refinement statistics are shown in Table 1.

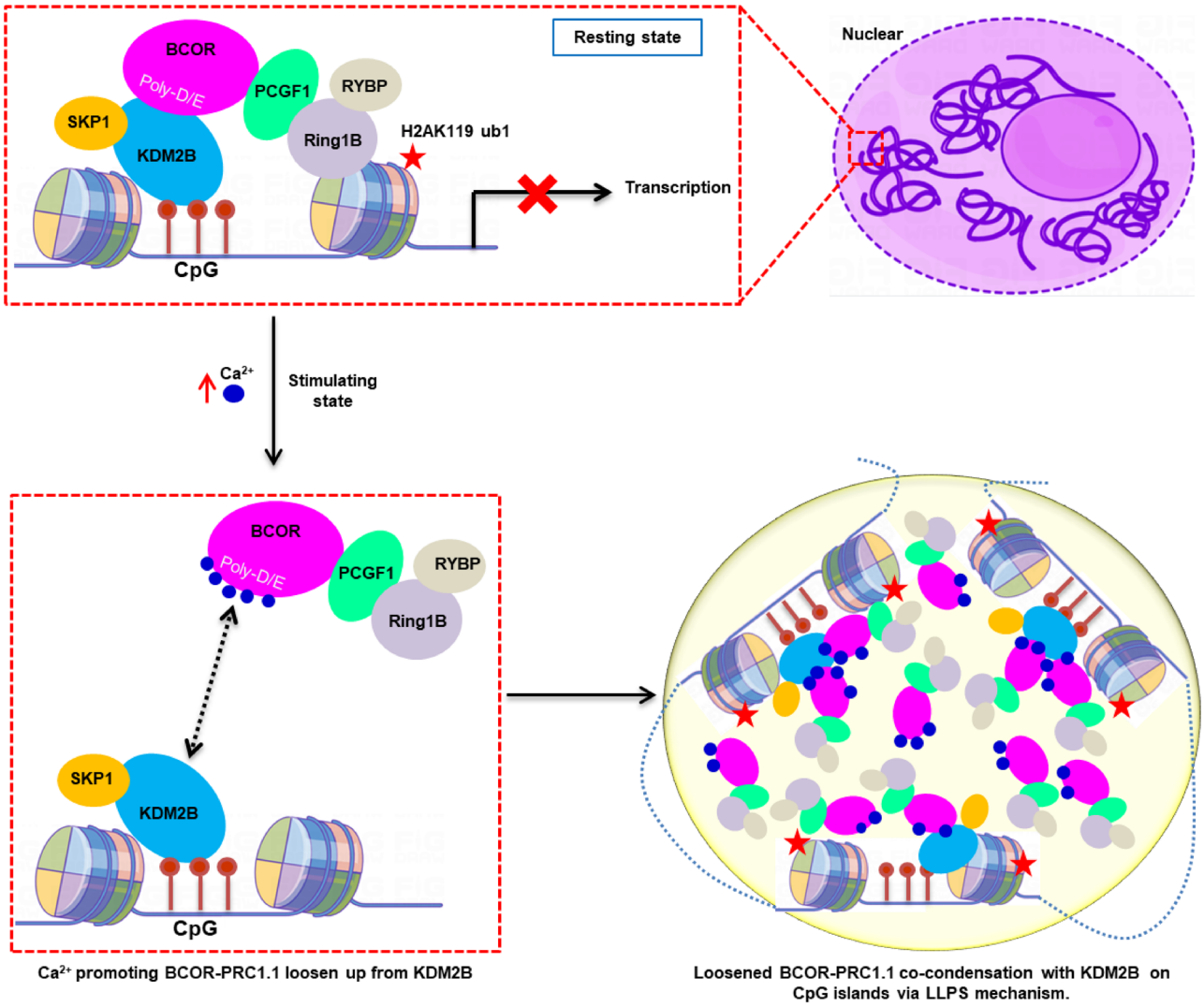

Fig. 7 | Proposed mechanisms on calcium ion modulating KDM2B recruitment enzymatic core of BCOR-PRC1.1 to CpG islands. In resting state, BCOR-PRC1.1 was recruited to CpG islands through interaction with KDM2B, leading to gene silence. After stimulation, concentration of nuclear Ca^{2+} is elevated. The elevated Ca^{2+} weakens the association between BCOR/PCGF1 and KDM2B, through neutralizing highly acidic Poly-D/E regions on linker of BCOR. Ca^{2+} also induces phase separation of BCOR/PCGF1. The elevated Ca^{2+} further promotes co-condensation of enzymatic core of BCOR-PRC1.1 with KDM2B on target loci via LLPS mechanism.

Cross-linking mass spectrometry (XL-MS)

$BCOR^{ANK\text{-}linker\text{-}PUFD}$/$PCGF1^{RAWUL}$/ $KDM2B^{F\text{-}box\text{-}LRRs}$/SKP1 complex was purified with Superdex 200 (GE) equilibrated against crosslinking buffer (20 mM HEPES pH 7.5, 150 mM NaCl). For cross-linking with bis[sulfosuccinimidyl] suberate (BS3), $BCOR^{ANK\text{-}linker\text{-}PUFD}$/$PCGF1^{RAWUL}$/$KDM2B^{F\text{-}box\text{-}LRRs}$/SKP1 complex (1 mg/mL) was reacted with 20-50 folds molar excess of BS^3 for 2 h at 4 °C, and reaction was quenched with Tris-base to final concentration of 50 mM and incubated for 15 min at room temperature. For cross-linking with 1-ethyl-3-[3-dimethylaminopropyl]carbodiimide hydrochloride (EDC), $BCOR^{ANK\text{-}linker\text{-}PUFD}$/$PCGF1^{RAWUL}$/ $KDM2B^{F\text{-}box\text{-}LRRs}$/SKP1 complex (1 mg/mL) was reacted with 10-30 folds molar excess of EDC for 1 h at room temperature. Cross-linking reaction was quenched with 50 mM Tris and 20 mM β-me, and incubated for 15 min at room temperature.

Crosslinked complexes were separated by SDS-PAGE, and stained by coomassie blue. Coomassie blue-stained gel bands were cut into small pieces and washed sequentially with water, 50 mM NH_4HCO_3 in 50% acetonitrile, and 100% acetonitrile. Disulfide bonds of the protein were reduced with 10 mM TCEP in 100 mM NH_4HCO_3 for 30 min at room temperature and followed by 55 mM iodoacetamide treatment in 100 mM NH_4HCO_3 for 30 min at room temperature in the dark. Then, the gel pieces were washed sequentially with 100 mM NH_4HCO_3 and 100% acetonitrile, and dried using a SpeedVac. Samples were then digested with trypsin (12.5 ng/μL) in 50 mM NH_4HCO_3 for 16 h at 37 °C, and the peptides were extracted twice with 50% acetonitrile/5% formic acid. The sample was evaporated to dryness, and resuspended with 0.1% formic acid, and desalted using MonoSpin™ C18 column, and then dried with SpeedVac.

The crosslinked peptides were then analyzed by liquid chromatography tandem mass spectrometry (LC-MS/MS) using an Easy-nLC 1200 nano HPLC, and the temperature of the analytical column was set to 55 °C during the experiment. Data-dependent tandem mass spectrometry (MS/MS) analysis was performed with a Q Exactive Orbitrap mass spectrometer. The crosslinked peptides were identified using pLink2 software (pFind Team, Beijing, China) as described previously[63,64]. Carbamidomethylation of cysteine was set as fixed modification, and oxidation of methionine was set as variable modification.

Small-Angel X-ray scattering (SAXS) data collection and processing

The small angle X-ray scattering data were obtained at the BL19U2 beamline of National center for Protein Science Shanghai (NCPSS) and

Table 1 | Data collection and refinement statistics

Data collection	
Space group	$P4_32_12$
Cell dimensions	
a, *b*, *c* (Å)	67.29, 67.29, 252.04
Resolution (Å)	126.02-2.20 (2.27-2.20)[a]
Total observations	421860 (37997)
Unique refection	30637 (2605)
R_{merge}	0.114 (1.180)
R_{pim}	0.045 (0.453)
$I / \sigma I$	12.0 (2.4)
Completeness (%)	100.0 (99.9)
Redundancy	13.8 (14.6)
Refinement	
Resolution (Å)	65.01-2.20
No. reflections	29020
R_{work} / R_{free} (%)[b]	20.02/23.84
No. atoms	
Protein	3522
Solvent	70
Average *B*-factors	
Protein	67.76
Solvent	59.84
R.m.s. deviations	
Bond lengths (Å)	0.005
Bond angles (°)	1.17
Ramachandran (%)	
Most favored	98.13
Allowed	1.87
Outlier	0.00

[a]The values in parentheses refer to statistics in the highest bin.
[b]Rfactor = $\sum(|Fobs| - k|Fcalc|)/\sum|Fobs|$; Rfree is the *R*-value for a test set of reflections consisting of a random 5% of the diffraction data not used in refinement.

Shanghai Synchrotron Radiation Facility (SSRF). SAXS data were collected from 100 μL of BCOR$^{ANK\text{-}linker\text{-}PUFD}$/PCGF1^{RAWUL}/KDM2B$^{F\text{-}box\text{-}LRRs}$/SKP1 hetero-tetramer or BCOR^{N1607}/PCGF1^{RAWUL}/KDM2B$^{F\text{-}box\text{-}LRRs}$/SKP1 hetero-tetramer loaded onto Superdex 200 Increase 10/300 GL column equilibrated with 20 mM Tris-HCl pH 7.5, 150 mM NaCl. Scattering data were averaged, scaled and background-corrected using software BioXTAS RAW. ATSAS program suite (version 3.1) was used for further process of SAXS data. GNOM software was used to calculate the pair distances distribution function *P(γ)* and maximum diameter (D_{max}). Ab initio modeling was carried out using the software GASBOR. 40 independent GASBOR models of each complex were averaged using DAMAVER. SAXS parameters were shown in Supplementary table 4.

Model building for BCOR^{N1607}/PCGF1^{RAWUL}/KDM2B$^{F\text{-}box\text{-}LRRs}$/SKP1 hetero-tetramer and BCOR$^{ANK\text{-}linker\text{-}PUFD}$/PCGF1^{RAWUL}/KDM2B$^{F\text{-}box\text{-}LRRs}$/SKP1 hetero-tetramer

To build structure model of BCOR^{N1607}/PCGF1^{RAWUL}/KDM2B$^{F\text{-}box\text{-}LRRs}$/SKP1 hetero-tetramer, software FoXSDock[65,66] was employed to dock BCOR^{PUFD} (1634–1746)/PCGF1^{RAWUL} dimer (isolated from our crystal structure of BCOR^{N1607}/PCGF1^{RAWUL}/KDM2B^{LRRs}) onto KDM2B$^{F\text{-}box\text{-}LRRs}$/SKP1 (PDB code 5JH5) with SAXS profile of the complex. Top ranked poses were collected for further analysis. Section of N1619-D1625 was generated from crystal structure of BCOR^{N1607} /PCGF1^{RAWUL}/KDM2B^{LRRs} heterotrimer. Then, modeling of the remaining residues E1607-A1618 and Q1626-S1633 from BCOR linker was performed using online software ModLoop[67].

For the modeling of BCOR$^{ANK\text{-}linker\text{-}PUFD}$/PCGF1^{RAWUL}/KDM2B$^{F\text{-}box\text{-}LRRs}$/SKP1 hetero-tetramer, ANK domain predicted by AlphaFold2 was docked on model structure of BCOR^{N1607} /PCGF1^{RAWUL}/KDM2B^{LRRs} using FoXSDock, with the SAXS profile of the complex and distance constraints based on cross-linking data with EDC cross-linker. For the distance constraints, the distance between Cα atom of E1484 from BCOR-ANK domain (residues 1461–1606) and Cα atom of K121 from SKP1 was set to 0-20 Å, and the distance between Cα atom of D1555 from BCOR-ANK domain and Cα atom of K142 from SKP1 was set to 0-20 Å. The linker of BCOR was further completed with software ModLoop.

Biolayer Interferometry Assay (BLI)

The inhibitory potency of calcium ion against BCOR$^{ANK\text{-}linker\text{-}PUFD}$/PCGF1^{RAWUL} dimer interaction with KDM2B$^{F\text{-}box\text{-}LRRs}$/SKP1 dimer was evaluated by the Octet R8 (Sartorius) using the bio-layer interferometry approach. Purified BCOR$^{ANK\text{-}linker\text{-}PUFD}$/PCGF1^{RAWUL} dimer was labeled with biotin and diluted with the buffer (20 mM HEPES pH8.0, 150 mM NaCl, 0.02% Tween 20) to 10 μg/mL and loaded onto a streptavidin biosensor (SAX). KDM2B$^{F\text{-}box\text{-}LRRs}$/SKP1 dimer (333 nM) acts as the mobile phase, in the presence or absence of calcium ion.

DIC and fluorescent imaging for LLPS in solution

All the LLPS samples of BCOR$^{ANK\text{-}linker\text{-}PUFD}$/PCGF1^{RAWUL} and mutant BCOR$^{ANK\text{-}linker\text{-}PUFD}$ (Poly-D/E^{3rd} to Poly-A)/PCGF1^{RAWUL} were prepared in the buffer containing 20 mM Tris pH 7.5, 150 mM NaCl and 0.5 mM TCEP. For Differential interference contrast (DIC) imaging of LLPS, the samples were loaded onto a glass slide and images were acquired on a Leica DM4B microscope. For fluorescence imaging of BCOR$^{ANK\text{-}linker\text{-}PUFD}$/PCGF1^{RAWUL}, KDM2B$^{F\text{-}box\text{-}LRRs}$/SKP1 and mutant KDM2B$^{F\text{-}box\text{-}LRRs}$ (K1137D/K1138D/R1147D)/SKP1, BCOR$^{ANK\text{-}linker\text{-}PUFD}$ was tagged with GFP at N-terminal, and SKP1 was tagged with mCherry at C-terminal. The samples were loaded onto a glass bottom culture dish. Imaging was performed with Zeiss LSM 800 Confocal Laser Scanning Microcopy.

Fluorescence recovery after photobleaching (FRAP) assay

The LLPS sample of BCOR$^{ANK\text{-}linker\text{-}PUFD}$/PCGF1^{RAWUL} (100 μM) induced by 5 mM $CaCl_2$ was papered for FRAP assay. The FRAP assay was performed using the FRAP module of a Leica SP8 X STED Laser Scanning Confocal Microscopy with a 100 x objective (oil immersion). The fluorescent labeled assemblies were bleached using laser beam. Region of interest loop (ROI) was bleached with laser power of 30% and exposure time 30 ms and recovery was imaged at low laser intensity with power of 10%. After photobleaching, images were continuously captured (1 image/5 s). Data from three independent experiments were used for analysis.

Imaging LLPS in live cells

cDNA encoding BCOR$^{ANK\text{-}linker\text{-}PUFD}$ (wild type or mutant) and PCGF1^{RAWUL} were cloned into vector pCDNA3.1 with EGFP-tag and mCherry-tag at the C-terminal, respectively. HeLa cells were seeded at 2×10^5 in a 6-well glass bottom culture plate, the plasmid pCDNA3.1-BCOR$^{ANK\text{-}linker\text{-}PUFD}$ (wild type or mutant)-EGFP (2 μg) and pCDNA3.1-PCGF1^{RAWUL}-mCherry (2 μg) were co-transfected with PEI after 18 h. Cells were transfected for 36 h before proceeding with subsequent live imaging. Imaging was performed with Zeiss LSM 800 Confocal Laser Scanning Microcopy.

Co-localization assay for BCOR, PCGF1 and KDM2B

cDNA encoding BCOR, PCGF1 and KDM2B were cloned into vector pCDNA3.1 with C-terminal mCherry-tag, ECFP-tag and EGFP-tag, respectively. The plasmids were co-transfected into HeLa cell with Lipo2000. After transfected for 36 h, imaging was performed with confocal microscope (Leica SP8 X STED).

Construct shRNA targeting BCOR

To knockdown endogenous BCOR in HEK293T cells, shRNA (5′ GGCACTTGGTGATATAACTCTCGAGA GTTATATCACCAAGTG CC3′) targeting the 3'-UTR of BCOR was constructed to pLKO.1 vector. shluc (5′ CCTAAGGTTAAGTCGCCCTCGCTCGAGCGAGGGC-GACTTAACCTTAGG 3′) targeting luciferase was set as negative control. Constitutive expression of shRNA was performed by lentiviral infection of the pLKO.1 vector with puromycin (2.5 μg/ml) selection. Knockdown efficiency was validated by western blot (anti-BCOR, 1:500, Mouse, Sigma-SAB4200843) and RT-qPCR. The primers used in qPCR were: forward 5′ TATGCAGATTCCAGTCAGCTC 3′, and reverse 5′ GGGCTGAATTTGCACATCTC 3′.

Subcellular fractionation isolation

Cell pellets were homogenized on ice in Buffer A (10 mM HEPES pH 8.0, 10 mM KCl, 1.5 mM $MgCl_2$, 0.34 M sucrose, 10% glycerol, 0.2% NP-40 (v/v), 1 x protease inhibitor cocktail) and nuclei were collected by centrifugation (2500 g for 10 min at 4 °C) and washed with Buffer B (Buffer A without NP-40). The collected supernatant was used as the cytoplasmic fraction and the pellets were the total nuclear. Then, the nuclear pellets were lysed in Buffer C (3 mM EDTA, 2 mM EGTA, inhibitors) for 30 min at 4 °C, and the nuclear soluble fractions were separated from the tight chromatin pellets by centrifugation (14,000 g for 10 min at 4 °C). The tight chromatin pellets were lysed with 4% SDS as chromatin fraction and H3 immunoblotting served as chromatin fraction control.

Gene expression analysis

HEK293T cells were grown on six-well plates (300,000 cells/ well) and cultured to 70%–80% density to conduct gene transfection. The 1 μg plasmid of BCOR (WT or WFY/A mutant) was transfected into the HEK293T cells that endogenous BCOR was knockdown by shBCOR. The empty vector (control) was transfected into sh-luc and sh-BCOR cells. Cells were collected after 48 h and total RNA was extracted with Trizol and chloroform, and quantified by nanodrop. 2.5 μg of total RNA was reverse to generate cDNA. Resultant cDNA was diluted 20-fold for RT-qPCR reaction. Reactions were run on a CFX96 instrument using 2 x RealStar Fast SYBR qPCR Mix (GenStar).Statistical significance was analyzed according to unpaired student's *t*-test.

Statistics and reproducibility

Isothermal titration calorimetry experiments and Gene expression analysis were repeated for three times. Co-immunoprecipitation and subcellular fractionation isolation experiments were repeated for two or three times. Statistical analyses were performed using GraphPad Prism 7 software.

Reporting summary

Further information on research design is available in the Nature Portfolio Reporting Summary linked to this article.

Data availability

Atomic coordinates and structure factors amplitudes have been deposited into Protein Data Bank with accession code (8HCU). Small-angle neutron scattering (SANS) datasets and models for $BCOR^{linker(N1607)\text{-}PUFD}$/$PCGF1^{RAWUL}$/$KDM2B^{F\text{-}box\text{-}LRRs/SKP1}$ hetero-tetramer and $BCOR^{ANK\text{-}linker\text{-}PUFD}$/$PCGF1^{RAWUL}$/$KDM2B^{F\text{-}box\text{-}LRRs}$/SKP1 hetero-tetramer were deposited to Small-Angle Scattering Biological Data Bank (SASBDB), with entry number SASDS67 and SASDS66, respectively. Replicated ITC data is available in Supplementary Data 1. Replicated WB data is available in Supplementary Data 2. Uncropped western blot images are available in Supplementary Data 3. The source data for the graphs presented in the figures of this paper are available in Supplementary Data 4.

Received: 23 January 2024; Accepted: 31 August 2024;
Published online: 10 September 2024

References

1. Jaenisch, R. & Bird, A. Epigenetic regulation of gene expression: how the genome integrates intrinsic and environmental signals. *Nat. Genet.* **33**, 245–254 (2003).
2. Kouzarides, T. Chromatin modifications and their function. *Cell* **128**, 693–705 (2007).
3. Blackledge, N. P. & Klose, R. J. The molecular principles of gene regulation by polycomb repressive complexes. *Nat. Rev. Mol. Cell Biol.* **22**, 815–833 (2021).
4. Jaenisch, R. & Young, R. Stem cells, the molecular circuitry of pluripotency and nuclear reprogramming. *Cell* **132**, 567–582 (2008).
5. Margueron, R. & Reinberg, D. The polycomb complex PRC2 and its mark in life. *Nature* **469**, 343–349 (2011).
6. Sparmann, A. & van Lohuizen, M. Polycomb silencers control cell fate, development and cancer. *Nat. Rev. Cancer* **6**, 846–856 (2006).
7. Schuettengruber, B., Bourbon, H. M., Di Croce, L. & Cavalli, G. Genome regulation by polycomb and trithorax: 70 years and counting. *Cell* **171**, 34–57 (2017).
8. Simon, J. A. & Kingston, R. E. Occupying chromatin: polycomb mechanisms for getting to genomic targets, stopping transcriptional traffic, and staying put. *Mol. Cell* **49**, 808–824 (2013).
9. Barbour, H., Daou, S., Hendzel, M. & Affar, E. B. Polycomb group-mediated histone H2A monoubiquitination in epigenome regulation and nuclear processes. *Nat. Commun.* **11**, 5947 (2020).
10. Hojfeldt, J. W. et al. Accurate H3K27 methylation can be established de novo by SUZ12-directed PRC2. *Nat. Struct. Mol. Biol.* **25**, 225–232 (2018).
11. Margueron, R. et al. Ezh1 and Ezh2 maintain repressive chromatin through different mechanisms. *Mol. Cell* **32**, 503–518 (2008).
12. Chittock, E. C., Latwiel, S., Miller, T. C. & Muller, C. W. Molecular architecture of polycomb repressive complexes. *Biochem. Soc. Trans.* **45**, 193–205 (2017).
13. Gao, Z. et al. PCGF homologs, CBX proteins, and RYBP define functionally distinct PRC1 family complexes. *Mol. Cell* **45**, 344–356 (2012).
14. Aranda, S., Mas, G. & Di Croce, L. Regulation of gene transcription by polycomb proteins. *Sci. Adv.* **1**, e1500737 (2015).
15. Gil, J. & O'Loghlen, A. PRC1 complex diversity: where is it taking us? *Trends Cell Biol.* **24**, 632–641 (2014).
16. Fursova, N. A. et al. Synergy between variant PRC1 complexes defines polycomb-mediated gene repression. *Mol. Cell* **74**, 1020–1036 e8 (2019).
17. Taherbhoy, A. M., Huang, O. W. & Cochran, A. G. BMI1-RING1B is an autoinhibited RING E3 ubiquitin ligase. *Nat. Commun.* **6**, 7621 (2015).
18. Zhu, Y. et al. Functional redundancy among polycomb complexes in maintaining the pluripotent state of embryonic stem cells. *Stem. Cell Rep.* **17**, 1198–1214 (2022).
19. Aldera, A. P. & Govender, D. Gene of the month: BCOR. *J. Clin. Pathol.* **73**, 314–317 (2020).
20. He, J. et al. Kdm2b maintains murine embryonic stem cell status by recruiting PRC1 complex to CpG islands of developmental genes. *Nat. Cell Biol.* **15**, 373–384 (2013).
21. Isshiki, Y. et al. KDM2B in polycomb repressive complex 1.1 functions as a tumor suppressor in the initiation of T-cell leukemogenesis. *Blood Adv.* **3**, 2537–2549 (2019).
22. Wang, Z. et al. A non-canonical BCOR-PRC1.1 complex represses differentiation programs in human ESCs. *Cell Stem. Cell* **22**, 235–251 e9 (2018).
23. Tiacci, E. et al. The corepressors BCOR and BCORL1: two novel players in acute myeloid leukemia. *Haematologica* **97**, 3–5 (2012).
24. van den Boom, V. et al. Non-canonical PRC1.1 targets active genes independent of H3K27me3 and is essential for leukemogenesis. *Cell Rep* **14**, 332–346 (2016).

25. Lempiainen, J. K. et al. BCOR-coupled H2A monoubiquitination represses a subset of androgen receptor target genes regulating prostate cancer proliferation. *Oncogene* **39**, 2391–2407 (2020).
26. Deaton, A. M. & Bird, A. CpG islands and the regulation of transcription. *Genes Dev.* **25**, 1010–1022 (2011).
27. Farcas, A. M. et al. KDM2B links the Polycomb Repressive Complex 1 (PRC1) to recognition of CpG islands. *Elife* **1**, e00205 (2012).
28. Wu, X., Johansen, J. V. & Helin, K. Fbxl10/Kdm2b recruits polycomb repressive complex 1 to CpG islands and regulates H2A ubiquitylation. *Mol. Cell* **49**, 1134–1146 (2013).
29. Xie, W. et al. Epigenomic analysis of multilineage differentiation of human embryonic stem cells. *Cell* **153**, 1134–1148 (2013).
30. Saxonov, S., Berg, P. & Brutlag, D. L. A genome-wide analysis of CpG dinucleotides in the human genome distinguishes two distinct classes of promoters. *Proc. Natl Acad. Sci. USA* **103**, 1412–1417 (2006).
31. Schaefer, E. J. et al. BCOR and BCORL1 mutations drive epigenetic reprogramming and oncogenic signaling by unlinking PRC1.1 from target genes. *Blood Cancer Discov.* **3**, 116–135 (2022).
32. Wong, S. J. et al. KDM2B recruitment of the polycomb group complex, PRC1.1, requires cooperation between PCGF1 and BCORL1. *Structure* **24**, 1795–1801 (2016).
33. Wong, S. J. et al. Structure and role of BCOR PUFD in noncanonical PRC1 assembly and disease. *Biochemistry* **59**, 2718–2728 (2020).
34. Boulard, M., Edwards, J. R. & Bestor, T. H. FBXL10 protects polycomb-bound genes from hypermethylation. *Nat. Genet.* **47**, 479–485 (2015).
35. Sportoletti, P., Sorcini, D. & Falini, B. BCOR gene alterations in hematologic diseases. *Blood* **138**, 2455–2468 (2021).
36. de Miranda, M. C. et al. Epidermal growth factor (EGF) triggers nuclear calcium signaling through the intranuclear phospholipase Cdelta-4 (PLCdelta4). *J. Biol. Chem.* **294**, 16650–16662 (2019).
37. Alonso, M. T. & Garcia-Sancho, J. Nuclear Ca(2+) signalling. *Cell Calcium* **49**, 280–289 (2011).
38. Kunrath-Lima, M. et al. Phospholipase C delta 4 (PLCdelta4) is a nuclear protein involved in cell proliferation and senescence in mesenchymal stromal stem cells. *Cell Signal* **49**, 59–67 (2018).
39. Chun, J.T., Santella, L. & Miller, J.J. Calcium | intracellular calcium waves. In *Encyclopedia of Biological Chemistry III* (ed. Jez, J.) 669–677 (Elsevier, 2021).
40. Vernon, R.M. et al. Pi-Pi contacts are an overlooked protein feature relevant to phase separation. *Elife* **7**, e31486 (2018).
41. Nakajima-Takagi, Y. et al. Polycomb repressive complex 1.1 coordinates homeostatic and emergency myelopoiesis. *eLife* **12**, e83004 (2023).
42. Sato, K., Fukami, Y. & Stith, B. J. Signal transduction pathways leading to Ca2+ release in a vertebrate model system: lessons from Xenopus eggs. *Semin Cell Dev. Biol.* **17**, 285–292 (2006).
43. Monteith, G. R., Prevarskaya, N. & Roberts-Thomson, S. J. The calcium-cancer signalling nexus. *Nat. Rev. Cancer* **17**, 367–380 (2017).
44. So, C. L., Saunus, J. M., Roberts-Thomson, S. J. & Monteith, G. R. Calcium signalling and breast cancer. *Semin. Cell Dev. Biol.* **94**, 74–83 (2019).
45. Izquierdo-Torres, E., Hernandez-Oliveras, A., Fuentes-Garcia, G. & Zarain-Herzberg, A. Calcium signaling and epigenetics: a key point to understand carcinogenesis. *Cell Calcium* **91**, 102285 (2020).
46. Shi, X. et al. Ca2+ regulates T-cell receptor activation by modulating the charge property of lipids. *Nature* **493**, 111–115 (2013).
47. Berridge, M. J., Bootman, M. D. & Roderick, H. L. Calcium signalling: dynamics, homeostasis and remodelling. *Nat. Rev. Mol. Cell Biol.* **4**, 517–529 (2003).
48. Snoeck, H. W. Calcium regulation of stem cells. *EMBO Rep.* **21**, e50028 (2020).
49. Clapham, D. E. Calcium signaling. *Cell* **131**, 1047–1058 (2007).
50. Wang, L. et al. Histone modifications regulate chromatin compartmentalization by contributing to a phase separation mechanism. *Mol. Cell* **76**, 646–659 e6 (2019).
51. Sanulli, S. et al. HP1 reshapes nucleosome core to promote phase separation of heterochromatin. *Nature* **575**, 390–394 (2019).
52. Zhang, H. et al. Liquid-liquid phase separation in biology: mechanisms, physiological functions and human diseases. *Sci. China Life Sci.* **63**, 953–985 (2020).
53. Pirrotta, V. & Li, H. B. A view of nuclear polycomb bodies. *Curr. Opin. Genet. Dev.* **22**, 101–109 (2012).
54. Eeftens, J. M., Kapoor, M. & Brangwynne, C. P. Epigenetic memory as a time integral over prior history of polycomb phase separation. *bioRvix* https://doi.org/10.1101/2020.08.19.254706 (2020).
55. Guo, Y., Zhao, S. & Wang, G. G. Polycomb gene silencing mechanisms: PRC2 chromatin targeting, H3K27me3 'readout', and phase separation-based compaction. *Trends Genet.* **37**, 547–565 (2021).
56. Plys, A. J. et al. Phase separation of polycomb-repressive complex 1 is governed by a charged disordered region of CBX2. *Genes Dev.* **33**, 799–813 (2019).
57. Fox, C. H. et al. A method for measuring intracellular free magnesium concentration in platelets using flow cytometry. *Magnes Res.* **20**, 200–207 (2007).
58. Maat, H. et al. The USP7-TRIM27 axis mediates non-canonical PRC1.1 function and is a druggable target in leukemia. *iScience* **24**, 102435 (2021).
59. Zhang, W.-Z. et al. The protein complex crystallography beamline (BL19U1) at the shanghai synchrotron radiation facility. *Nuclear Sci. Tech.* **30**, 170 (2019).
60. Evans, P. R. An introduction to data reduction: space-group determination, scaling and intensity statistics. *Acta. Crystallogr. D Biol. Crystallogr.* **67**, 282–292 (2011).
61. Lebedev, A. A., Vagin, A. A. & Murshudov, G. N. Model preparation in MOLREP and examples of model improvement using X-ray data. *Acta. Crystallogr. D Biol. Crystallogr.* **64**, 33–39 (2008).
62. Kovalevskiy, O., Nicholls, R. A., Long, F., Carlon, A. & Murshudov, G. N. Overview of refinement procedures within REFMAC5: utilizing data from different sources. *Acta. Crystallogr. D Struct. Biol.* **74**, 215–227 (2018).
63. Yang, B. et al. Identification of cross-linked peptides from complex samples. *Nat. Methods* **9**, 904–906 (2012).
64. Lu, S. et al. Mapping native disulfide bonds at a proteome scale. *Nat. Methods* **12**, 329–331 (2015).
65. Schneidman-Duhovny, D., Hammel, M. & Sali, A. Macromolecular docking restrained by a small angle X-ray scattering profile. *J. Struct. Biol.* **173**, 461–471 (2011).
66. Schneidman-Duhovny, D., Hammel, M., Tainer, J. A. & Sali, A. FoXS, FoXSDock and MultiFoXS: Single-state and multi-state structural modeling of proteins and their complexes based on SAXS profiles. *Nucleic Acids Res.* **44**, W424–W429 (2016).
67. Fiser, A., Do, R. K. & Sali, A. Modeling of loops in protein structures. *Protein Sci.* **9**, 1753–1773 (2000).

Acknowledgements

We thank the staff from BL19U1 and BL19U2 beamlines at National Facility for Protein Science in Shanghai (NFPS) and Shanghai Synchrotron Radiation Facility, for assistance during data collection. The work was financially supported by grants from the National Key Research and Development Program (2022YFA1303101, 2017YFA0504104), Guangdong Provincial Key Laboratory of Biocomputing (2016B030301007), and Key Laboratory of Regenerative Biology, Guangzhou Institutes of Biomedicine and Health, Chinese Academy of Sciences (KLRB202004)

Author contributions

J.X., J.L., and C.P. designed experiment. R.C., F.S., Y.Z., M.S., Y.D., Y.Y., and C.S. performed biochemical and cellular experiments. J.X., F.S., R.C., and J.L. performed structural studies. J.X., J.L., and R.C. wrote and edited the manuscript.

Competing interests

The authors declare no competing interests.

Additional information

Supplementary information The online version contains supplementary material available at https://doi.org/10.1038/s42003-024-06820-3.

Correspondence and requests for materials should be addressed to Jinsong Liu or Jinxin Xu.

Peer review information *Communications Biology* thanks the anonymous reviewers for their contribution to the peer review of this work. Primary Handling Editor: Christina Karlsson Rosenthal. A peer review file is available.